

## PHOTOMETRIC DETERMINATION OF THE MASS ACCRETION RATES OF PRE-MAIN SEQUENCE STARS. I. METHOD AND APPLICATION TO THE SN 1987A FIELD

GUIDO DE MARCHI,<sup>1</sup> NINO PANAGIA,<sup>2,3,4</sup> AND MARTINO ROMANIELLO<sup>5</sup>

*Accepted for publication in "The Astrophysical Journal"*

### ABSTRACT

We have developed and successfully tested a new self-consistent method to reliably identify pre-main sequence (PMS) objects actively undergoing mass accretion in a resolved stellar population, regardless of their age. The method does not require spectroscopy and combines broad-band  $V$  and  $I$  photometry with narrow-band  $H\alpha$  imaging to: (1) identify all stars with excess  $H\alpha$  emission; (2) convert the excess  $H\alpha$  magnitude into  $H\alpha$  luminosity  $L(H\alpha)$ ; (3) estimate the  $H\alpha$  emission equivalent width; (4) derive the accretion luminosity  $L_{\text{acc}}$  from  $L(H\alpha)$ ; and finally (5) obtain the mass accretion rate  $\dot{M}_{\text{acc}}$  from  $L_{\text{acc}}$  and the stellar parameters (mass and radius). By selecting stars with an accuracy of 15% or better in the  $H\alpha$  photometry, the statistical uncertainty on the derived  $\dot{M}_{\text{acc}}$  is typically  $\lesssim 17\%$  and is dictated by the precision of the  $H\alpha$  photometry. Systematic uncertainties, of up to a factor of 3 on the value of  $\dot{M}_{\text{acc}}$ , are caused by our incomplete understanding of the physics of the accretion process and affect all determinations of the mass accretion rate, including those based on a spectroscopic  $H\alpha$  line analysis.

As an application of our method, we study the accretion process in a field of 9.16 arcmin<sup>2</sup> around SN 1987A, using existing Hubble Space Telescope photometry. We identify as bona-fide PMS stars a total of 133 objects with a  $H\alpha$  excess above the  $4\sigma$  level and a median age of 13.5 Myr. Their median mass accretion rate of  $2.6 \times 10^{-8} M_{\odot} \text{ yr}^{-1}$  is in excellent agreement with previous determinations based on the  $U$ -band excess of the stars in the same field, as well as with the value measured for G-type PMS stars in the Milky Way. The accretion luminosity of these PMS objects shows a strong dependence on their distance from a group of hot massive stars in the field and suggests that the ultraviolet radiation of the latter is rapidly eroding the circumstellar discs around PMS stars.

*Subject headings:* accretion, accretion disks – stars: formation – stars: pre-main-sequence – Magellanic Clouds

### 1. INTRODUCTION

In the current star formation paradigm, low-mass stars grow in mass over time through accretion of matter from a circumstellar disc (e.g. Lynden-Bell & Pringle 1974; Appenzeller & Mundt 1989; Bertout 1989). This accretion process is believed to occur via the magnetic field lines that connect the star to its disc and that act as funnels for the gas (e.g. Königl 1991; Shu et al. 1994). The strong excess emission observed in most of these pre-main sequence (PMS) stars is believed to originate through gravitational energy, released by infalling matter, that ionises and excites the gas. Thus, the excess luminosity of these objects (the classical T Tauri stars) can be used to measure the mass accretion rate.

A reliable measurement of the rate of mass accretion onto PMS stars is of paramount importance for understanding the evolution of both the stars and their discs (see e.g. review by Calvet et al. 2000). Of particular interest is determining how the mass accretion rate changes with time as a star approaches its main sequence, whether it depends on the final mass of the forming star and whether it is affected by the chemical composition and density of its parent molecular cloud or by

the proximity of hot, massive stars.

Ground-based spectroscopic studies of nearby young star-forming regions (e.g. in Taurus, Auriga, Ophiuchus, Orion) show that the mass accretion rate appears to decrease steadily with time, from  $\sim 10^{-8} M_{\odot} \text{ yr}^{-1}$  at ages of  $\sim 1$  Myr to  $< 10^{-9} M_{\odot} \text{ yr}^{-1}$  at  $\sim 10$  Myr (Muzerolle et al. 2000; Sicilia-Aguilar et al. 2005; 2006). While at face value this is in line with the expected evolution of viscous discs (Hartmann et al. 1998), the scatter on the data is very large, exceeding 2 dex at any given age. This is at least in part explained by the recent finding that the mass accretion rate seems also to depend quite steeply on the mass of the forming star. Muzerolle et al. (2003; 2005), Natta et al. (2004; 2006), White & Hillenbrand (2004) and Sicilia-Aguilar et al. (2006) consistently report that the accretion rate  $\dot{M}_{\text{acc}}$  decreases with the stellar mass  $M$  as  $\dot{M}_{\text{acc}} \propto M^2$ , albeit with large uncertainties on the actual value of the power-law index. On the other hand, Clarke & Pringle (2006) warn that such a steep decline might be spurious and strongly driven by detection/selection thresholds.

While observational uncertainties and potential systematic errors may well contribute to the present uncertainty, the true limitation in this field of research currently comes from the paucity of available measurements. Indeed, all the results so far obtained are based on the mass accretion rates of a small number of stars (just over one hundred), all located in nearby Galactic star forming regions, covering a very limited range of ages and no appreciable range of metallicity (all clouds mentioned above having essentially solar metallicity; e.g. Padgett 1996).

The origin of this limitation is to be found in the technique used to measure PMS mass accretion rates. Regardless as

<sup>1</sup> European Space Agency, Space Science Department, Keplerlaan 1, 2200 AG Noordwijk, Netherlands; gdemarchi@rssd.esa.int

<sup>2</sup> Space Telescope Science Institute, 3700 San Martin Drive, Baltimore, MD 21218, USA, panagia@stsci.edu

<sup>3</sup> INAF-CT, Osservatorio Astrofisico di Catania, Via S. Sofia 78, 95123 Catania, Italy

<sup>4</sup> Supernova Limited, VGV #131, Northsound Road, Virgin Gorda, British Virgin Islands

<sup>5</sup> European Southern Observatory, Karl-Schwarzschild-Str. 2, 85748 Garching, Germany

to whether the latter are derived from the analysis of veiling in the photospheric absorption lines (usually at ultraviolet and optical wavelengths) or through a detailed study of the profile and intensity of emission lines (usually  $H\alpha$ ,  $Pa\beta$  or  $Br\gamma$ ), these techniques typically require medium to high resolution spectroscopy for each individual object. Even with modern multi-object spectrographs at the largest ground-based telescopes, this approach is not very efficient and cannot reach beyond nearby star forming regions or the Orion cluster, as crowding and sensitivity issues rule out but the brightest objects in more distant regions like the centre of the Milky Way or the Magellanic Clouds. While in principle the PMS mass accretion rate can be estimated from the  $U$ -band excess if the spectral type is known (see e.g. Gullbring et al. 1998; Romaniello et al. 2004), this method is potentially subject to large uncertainties in the extinction and in the determination of the correct spectral type and effective temperature when spectroscopy is not available.

In order to overcome these limitations and significantly extend the sample of stars with a measured mass accretion rate, we have developed and successfully tested a new method to reliably measure  $\dot{M}_{acc}$  that does not require spectroscopy. The method, described in the following sections, combines broadband  $V$  and  $I$  photometry with narrow-band  $H\alpha$  imaging and allows us to identify all stars with excess  $H\alpha$  emission and to derive from it the accretion luminosity  $L_{acc}$  and hence  $\dot{M}_{acc}$  for hundreds of objects simultaneously.

The paper is organised as follows: in Section 2 we address the identification of PMS stars via their colour excess and in Section 3 we show how to reliably convert the measured excess into  $H\alpha$  luminosity and equivalent width. Section 4 shows how the accretion luminosity and mass accretion rate can be obtained from the  $H\alpha$  luminosity and Section 5 presents an application of the method to the field of SN 1987A, in the Large Magellanic Cloud (LMC). A thorough discussion of all systematic uncertainties involved in the method is provided in Section 6, while a general discussion and conclusions follow in Section 7. The Appendix provides additional figures and tabular material.

## 2. IDENTIFICATION OF PMS STARS THROUGH THEIR COLOUR EXCESS

One of the characteristic signatures of the accretion process on to PMS stars is the presence of excess emission in  $H\alpha$  (see Calvet et al. 2000). Although surveys to search for stars with  $H\alpha$  excess emission over large sky areas have been traditionally carried out via slitless spectroscopy (e.g. Herbig 1957; Kohoutek & Wehmeyer 1999), extensive studies in which narrow-band  $H\alpha$  imaging is combined with broadband photometry also exist (e.g. Parker et al. 2005; Drew et al. 2005).

Recently, Romaniello et al. (1998), Panagia et al. (2000) and Romaniello et al. (2006) used HST/WFPC2 photometry in  $H\alpha$  (F656N) and the R band (F675W) to provide the first direct detection of extra-galactic PMS stars with strong  $H\alpha$  emission in the LMC. Their approach is based on the widely adopted use of the R band magnitude as an indicator of the level of the photospheric continuum near the  $H\alpha$  line. Therefore, stars with strong  $H\alpha$  emission will have a large  $R-H\alpha$  colour. From the analysis of the specific F656N and F675W filter response curves of the WFPC2 instrument, Panagia et al. (2000) conclude that an equivalent width ( $W_{eq}$ ) of the  $H\alpha$  emission line in excess of  $8 \text{ \AA}$  will result in a colour excess  $R-H\alpha \gtrsim 0.3$ .

This way of identifying PMS stars is more accurate and reliable than the simple classification based on the position of the objects in the Hertzsprung–Russell diagram, i.e. stars placed well above the main sequence (e.g. Gilmozzi et al. 1994; Hunter et al. 1995; Nota et al. 2006; Gouliermis et al. 2007). The reason is twofold: (i) contamination by older field stars and the effects of differential extinction may lead to an overestimate of the actual number of candidate young, low-mass PMS stars, i.e. those “above” the MS; (ii) older PMS stars, already close to their MS, cannot be properly identified with this method, thereby resulting in an underestimate of the number of stars that are still forming. When PMS stars are identified by means of their  $R-H\alpha$  colour excess, both problems disappear.

Similarly, this approach is more practical, efficient and economical than slitless spectroscopy for studying PMS stars in dense star forming regions in the Milky Way and nearby galaxies, which are today accessible thanks to high-resolution observations, in particular those made with the HST.

We will show in Section 3 that the level of the photospheric continuum near  $H\alpha$  can be directly derived from the observed  $V$  and  $I$  magnitudes. This means that PMS stars with an  $H\alpha$  excess can be identified without actually measuring the canonical  $R-H\alpha$  index. On the other hand, since  $R-H\alpha$  has traditionally been used in PMS stars studies, we first show here how one can derive analytically the  $R$  magnitude of an object from the measured  $V$  and  $I$  magnitudes. In this way, we intend to make it possible for those who do not dispose of R-band photometry for their fields to derive it in an accurate way by using measurements in the neighbouring  $V$  and  $I$  bands. The latter are more commonly used than the R band in photometric studies of resolved stellar populations and are particularly popular among HST observers.

### 2.1. Deriving $R$ from $V$ and $I$

The absence of remarkable spectral features between  $5000 \text{ \AA}$  and  $9000 \text{ \AA}$  in the stellar continuum of dwarfs and giants with effective temperatures in the range  $4000 \text{ K} \lesssim T_{eff} \lesssim 10000 \text{ K}$  implies that their  $V-R$  and  $V-I$  colours depend primarily on the effective temperature of the stars and less on their metallicity. In effect,  $V-I$  remains a useful colour index for temperature determinations (von Braun et al. 1998; Bessell, Castelli & Plez 1998).

The colour–colour sequences in the  $UBVR IJ KLMN$  passbands published by Johnson (1966) revealed a very tight correlation between the mean  $V-R$  and  $V-I$  colours of local dwarfs and giants (see Figure 1). The correlation is remarkably linear in the range  $0 < V-I < 2$  (i.e.  $4000 \text{ K} \lesssim T_{eff} \lesssim 10000 \text{ K}$ ), where  $(V-R) = 0.58 \times (V-I)$  (dashed line in Figure 1), and it remains linear for  $2 < V-I < 4$  (i.e.  $3000 \text{ K} \lesssim T_{eff} \lesssim 4000 \text{ K}$ ), albeit with a shallower slope (0.45; dot-dashed line). It is, therefore, possible and meaningful to attempt to derive the value of the  $R$  magnitude from the knowledge of  $V$  and  $I$ , particularly because no extrapolation beyond the available wavelength range is involved. The simple inversion of the relationship above gives  $R = 0.42V + 0.58I$  for the system of Johnson.<sup>6</sup>

Interestingly, this relationship is very similar to the one that we would obtain if we assumed that the proportion with

<sup>6</sup> We note here that Johnson’s  $I$  is not the same as the much more commonly used Cousin’s  $I$ . Therefore, the colour relationships given here cannot be used for the Cousin system. Proper relationships for the most common magnitude systems are provided in the Appendix.

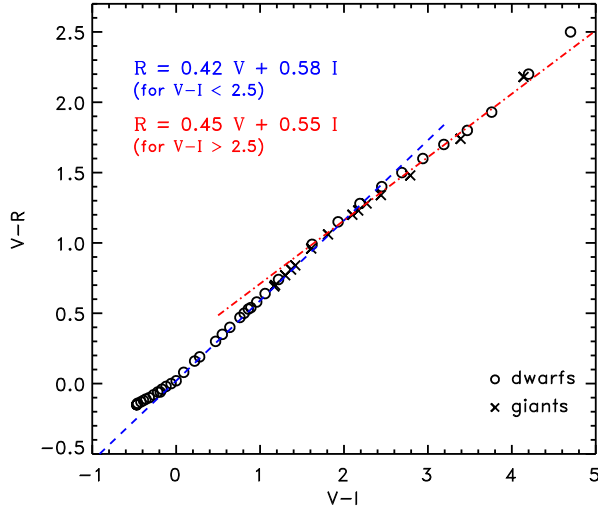


FIG. 1.— The tight correlation between  $V-R$  and  $V-I$  from the colour–colour sequences of Johnson (1966). Circles indicate dwarfs and crosses giants.

which the  $V$  and  $I$  magnitudes contribute to the  $R$  magnitude is simply dictated by the ratio of the effective wavelengths of the filters. The effective wavelengths of the  $V$ ,  $R$  and  $I$  bands in Johnson’s system are, respectively,  $\lambda_e^V = 5500 \text{ \AA}$ ,  $\lambda_e^R = 7000 \text{ \AA}$  and  $\lambda_e^I = 9000 \text{ \AA}$ , which imply that the  $V$  band should contribute for  $(7000 - 5500)/(9000 - 5500) \simeq 0.43$  and the  $I$  band for  $(9000 - 7000)/(9000 - 5500) \simeq 0.57$  to the  $R$ -band magnitude. These values are remarkably close to those observed.

The apparent disarming simplicity of this conclusion, however, should not lead one to think that this is the case for any photometric system. In particular, for spectral bands much wider than Johnson’s, such as some of the HST/WFPC2 and HST/ACS filters, the matter becomes more complicated because the true effective wavelength can depend significantly on the spectral properties of the source (i.e. its temperature). In these cases, the relationship should be derived via direct observations in the specific bands or through synthetic photometry, when the properties of the photometric system are well characterised.

Due to the large number of inter-related observing modes offered by the scientific instruments on board the HST, synthetic photometry has long been established as the most practical and efficient approach to their calibration (see Koornneef et al. 1986; Horne 1988; Sirianni et al. 2005). For this reason, reference tables exist that accurately describe the main optical components of the telescope and instruments as well as the response and quantum efficiency of the detectors as a function of wavelength. Therefore, thanks also to the availability of standardised software packages (e.g. Synphot; see Laidler et al. 2008), it is relatively easy to derive synthetic magnitudes from observed or theoretical stellar spectra for various HST instrumental configurations.

We have used both observed and theoretical stellar spectra, taken respectively from the Bruzual-Persson-Gunn-Stryker (BPGS) Spectrophotometry Atlas (see Gunn & Stryker 1983) and from the stellar atmosphere models of Bessell et al. (1998), to compute colour relationships between  $R$ -like magnitudes and  $V-I$ -like colours for various HST instruments and ground photometric systems. Details on how the colour trans-

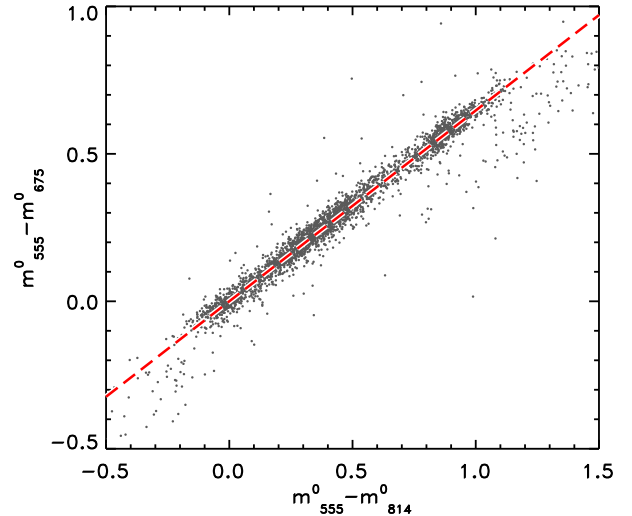


FIG. 2.— Colour–colour diagram of all stars in the SN 1987A field with combined mean photometric error  $\delta_3 \leq 0.05$  mag. The dashed line shows the colour relationship derived for the bands in question (F555W, F675W and F814W) from the models of Bessell et al. (1998) and is in excellent agreement with the observations.

formations were derived and a table of coefficients (Table 3) can be found in the Appendix, while a brief comparison with HST data is given in the following section.

## 2.2. Comparison with the data

To verify the validity of the predicted colour relationships, we have used WFPC2 photometry of a field around SN 1987A studied by Romaniello (1998), Panagia et al. (2000) and Romaniello et al. (2002). The observations cover a field of  $9.16 \text{ arcmin}^2$  and were collected over three epochs, namely 1994 September, 1996 February and 1997 July. The advantage of this catalogue is that the magnitude of each star in it is individually corrected for the effects of interstellar extinction by using the information provided simultaneously by all broad-band filters (see Romaniello et al. 2002 for more details). While it would be possible to include the effects of reddening in the calculations of the colour relationships of Table 3, it is more appropriate in this case to correct the observed magnitudes, since considerable differential extinction is likely to be present in this field (see Panagia et al. 2000; De Marchi & Panagia, in preparation).

From the catalogue of Romaniello et al. (2002), we have selected all those stars whose mean error  $\delta_3$  in the three bands F555W, F675W and F814W does not exceed 0.05 mag, where

$$\delta_3 = \sqrt{\frac{\delta_{555}^2 + \delta_{675}^2 + \delta_{814}^2}{3}} \quad (1)$$

and  $\delta_{555}$ ,  $\delta_{675}$  and  $\delta_{814}$  are the photometric uncertainties in each individual band after correction for interstellar extinction. A total of 9635 stars satisfy the condition set by Equation 1, out of 21955 objects in the complete catalogue.

The colour–colour diagram for the stars selected in this way is shown in Figure 2. The dashed line in that figure corresponds to the colour relationship derived for the bands in question from the models of Bessell et al. (1998; see the Appendix) and is practically indistinguishable from the best linear regression fit to the data, which has a slope of  $0.645 \pm 0.003$ . Although these models were selected to match

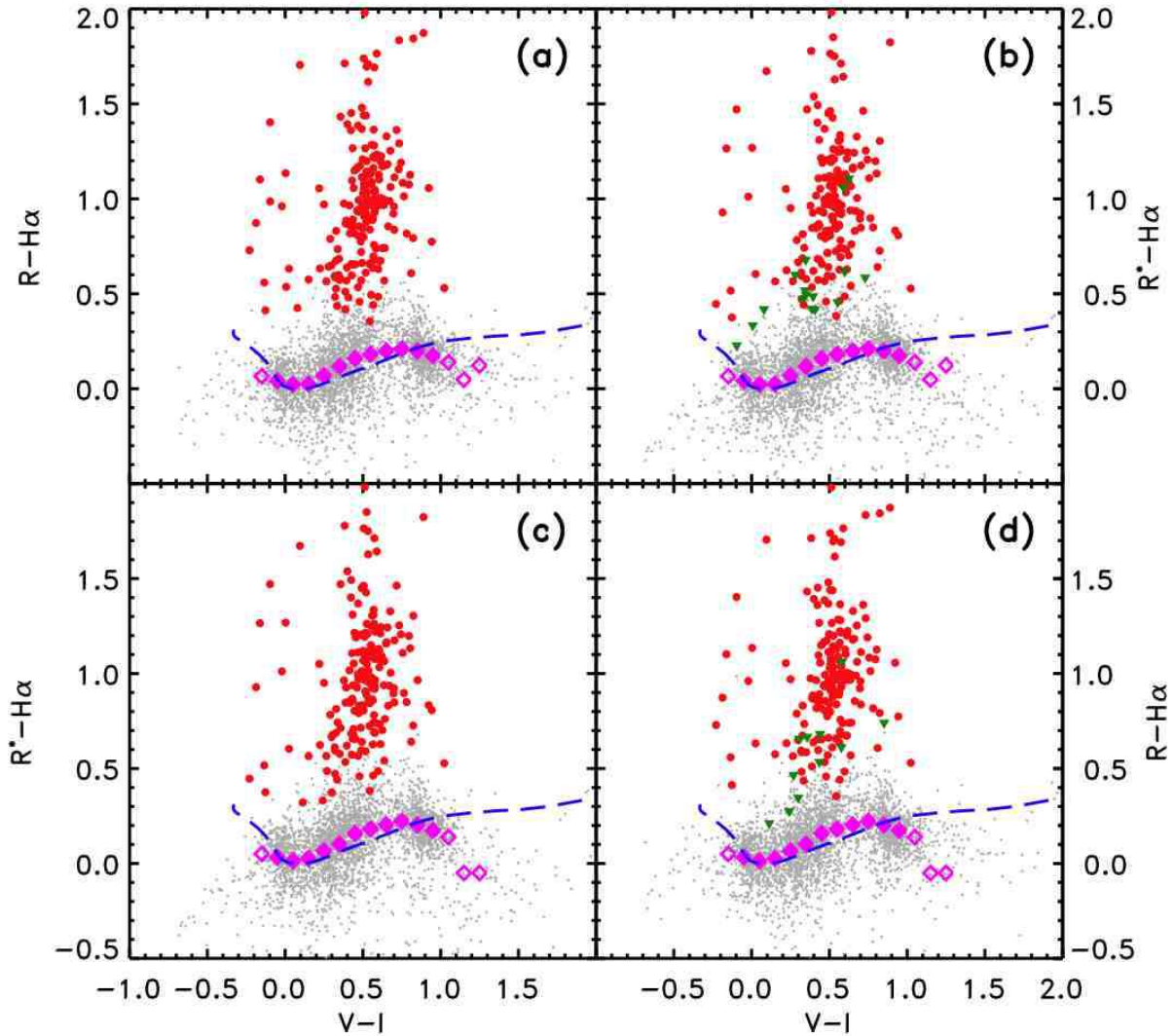


FIG. 3.— Comparison between the measured and derived  $R-H\alpha$  colour excess. While  $R$  denotes the magnitude actually measured in the F675W band,  $R^*$  indicates the magnitude derived from  $V$  (F555W) and  $I$  (F814W) by using the relationship of Table 3. Diamonds represent the measured average  $R-H\alpha$  colour of the population while the dashed lines is the colour predicted by theoretical models. Thick dots corresponds to stars with  $R-H\alpha$  excess larger than  $4\sigma$ . See text for an explanation of the remaining symbols.

the metallicity of the LMC, having used the relationship derived with the BPGS atlas or that for  $[M/H] = -1$  would have still resulted in a very good fit, within the observational uncertainties. This result confirms that, at least over the range explored here, metallicity does not play a dominant role in the colour relationships.

We provide a further proof of the reliability and accuracy of the interpolated R-band magnitudes in Figure 3, where we compare the identification of PMS stars based on the measured and interpolated  $R-H\alpha$  colour. To distinguish the observed from interpolated R-band magnitude, we indicate the latter with  $R^*$ , as explained below.<sup>7</sup> In this case, from the photometry of Romaniello et al. (2002) already corrected for reddening, we have further restricted the selection to objects with  $\delta_3 \leq 0.02$ , comprising 3241 stars.

Diamonds in Figure 3 represent the average  $R-H\alpha$  colour of the population and, as such, define the reference with re-

spect to which one should look for excess emission. The dashed lines represent the theoretical colour relationship obtained using the Bessell et al. (1998) model atmospheres mentioned above for normal main-sequence stars and is in rather good agreement with the average observed colours in the range  $-0.1 \lesssim V-I \lesssim 1$  (filled diamonds). The rms deviation between the model and the data over this range amounts to 0.03 mag and is dominated by the systematic departure in the range  $0.2 \lesssim V-I \lesssim 0.7$ . The latter could be due to a number of reasons, including the inability of the models to accurately describe the properties of the  $H\alpha$  line since they are meant to be used for broad-band photometry. The departure of the models from the data at  $V-I > 1$  stems from both small number statistics and the fact that the bulk of the population there comes from red giants, which have lower surface gravity and possibly lower metallicity than those assumed in the models. In the following, we will concentrate our analysis to the range  $-0.1 \lesssim V-I \lesssim 1$  marked by the filled diamonds.

Figure 3a is based on the observed data and we indicate as large dots all stars whose observed  $R-H\alpha$  colour exceeds the local average by at least four times the individual pho-

<sup>7</sup> Hereafter, we will use for simplicity the symbols  $V$ ,  $R$ ,  $I$  and  $H\alpha$  to indicate the respective WFPC2 bands. When differences between photometric systems are important (e.g. in Table 3), all bands will be indicated with their specific name.

tometric uncertainty in the colour, i.e. the one specific to each star. Consequently, these objects must be regarded as having a bona-fide  $H\alpha$  excess above the  $4\sigma$  level. There are 199 such objects in panel (a). In panel (b) we have replaced the observed  $R$  magnitude with its interpolated value  $R^*$ . All but 16 of the 199 stars with  $4\sigma$  excess in panel (a) have a  $4\sigma$  excess also in panel (b) and are indicated as large dots. The remaining 16 objects, marked as triangles, fail this requirement as their colour is closer to the local average colour than four times their specific combined photometric uncertainty.

In panels (c) and (d) we study the uncertainty in the other direction, i.e. from the interpolated to the observed plane. Panel (c) simulates the case in which, no  $R$ -band data being available, one uses the interpolated  $R^*$  value from Table 3 to identify stars with  $H\alpha$  excess emission. Stars indicated as large dots in panel (c) are those with interpolated  $R^* - H\alpha$  colour exceeding the local average by at least four times the individual photometric uncertainty in the colour, i.e. those with  $H\alpha$  excess above the  $4\sigma$  level. A total of 194 stars meet this condition. All but 11 of them would have met the  $4\sigma$  excess condition if we had used the actually observed  $R$ -band magnitude. They are indicated as large dots in panel (d), while the 11 objects failing the condition are marked as triangles.

From Figure 3 we can draw some quantitative conclusions on the statistical significance of the detection of the colour excess in  $H\alpha$ . First of all, it does not surprise that some objects detected as bona-fide  $H\alpha$  excess stars in panel (a) are rejected in panel (b), since the typical photometric uncertainty on  $R^*$  is a factor of  $\sqrt{2}$  higher than that on  $R$ , as one must combine the uncertainties on  $V$  and  $I$  that concur to the estimate of  $R^*$  (although the major contribution to the uncertainty on the  $R - H\alpha$  colour of a star comes from the  $H\alpha$  band). For the same reason, it is to be expected that panel (c) will yield less objects with bona-fide  $H\alpha$  excess than panel (a).

Considering the number of detections and mismatches of Figure 3, we estimate that using the interpolated  $R^*$  in place of  $R$  a fraction of  $(199 - 194)/199 = 2.5\%$  of the objects with  $H\alpha$  excess at the  $4\sigma$  level would be missing and that for about  $11/194 = 5.7\%$  of the detections the assigned statistical significance would be higher than indicated by direct  $R$  measurements. We conclude that our interpolation scheme is quite reliable in that it can provide the correct identification of PMS stars in no less 94% of the cases.

### 3. QUANTIFYING THE EXCESS $H\alpha$ EMISSION: FROM COLOUR EXCESS TO LINE LUMINOSITY AND EQUIVALENT WIDTH

While helpful to accurately identify PMS stars, the  $R - H\alpha$  colour excess alone does not immediately provide an absolute measure of the  $H\alpha$  luminosity  $L(H\alpha)$  nor of the equivalent width  $W_{\text{eq}}(H\alpha)$ , which are necessary to arrive at the mass accretion rate. In order to measure  $L(H\alpha)$ , one needs a solid estimate of the stellar spectrum in the  $H\alpha$  band (i.e. without the contribution of the emission). Similarly, to measure  $W_{\text{eq}}(H\alpha)$ , a solid estimate of the level of the stellar continuum inside the  $H\alpha$  band is needed. Since the  $R$  band is over an order of magnitude wider than the  $H\alpha$  filter, it cannot provide this information accurately, but only gives a rough estimate of the continuum level. In this section we present a simple method that allows us to measure  $L(H\alpha)$  for the objects with an  $H\alpha$  excess and to derive the level of their spectral continuum inside the  $H\alpha$  band, determining in this way also  $W_{\text{eq}}(H\alpha)$ .

#### 3.1. The $H\alpha$ line luminosity

The method is based on the simple consideration that, at any time, the largest majority of stars of a given effective temperature  $T_{\text{eff}}$  in a stellar population will have no excess  $H\alpha$  emission. Therefore, for stars of that effective temperature, the *average* value of a colour index involving  $H\alpha$  (for instance  $V - H\alpha$ , and thus not just  $R - H\alpha$ ) effectively defines a spectral reference template with respect to which the  $H\alpha$  colour excess should be sought. Note that this is not only true for populations comprising both young and old stars, such as those typical of extragalactic stellar fields, but also for very young populations since PMS objects show large variations in their  $H\alpha$  emission over hours or days (e.g. Fernandez et al. 1995; Smith et al. 1999; Alencar et al. 2001), with only about one third of them at any given time being active  $H\alpha$  emitters above a  $W_{\text{eq}}(H\alpha) \simeq 10 \text{ \AA}$  threshold (Panagia et al. 2000).

To better clarify the working of our method, we display in Figure 4 the  $V - H\alpha$  colour as a function of  $V - I$  for a set of stars taken from the catalogue of Romaniello et al. (2002). This time, we have selected a total of 4156 stars, namely all objects with  $\delta_3 \leq 0.1$  mag, where the mean uncertainty  $\delta_3$  is defined as in Equation 1, but for the  $V$ ,  $I$  and  $H\alpha$  bands instead of  $V$ ,  $I$  and  $R$ . Therefore, no  $R$ -band information is used in this case and, in fact, no  $R$ -band data is needed. It should be noted that  $\delta_3$  is dominated by the uncertainty on the  $H\alpha$  magnitude, while the median value of the uncertainty in the other two bands is  $\delta_V = 0.014$  and  $\delta_I = 0.016$ , respectively.

The thick dashed line in Figure 4 represents the average  $V - H\alpha$  colour obtained as the running median with a box-car size of 100 points. The thin solid line shows the colours in these filters for the model atmospheres of Bessell et al. (1998) mentioned above (note again the  $< 0.1$  mag discrepancy between models and observations around  $V - I \simeq 0.6$ , most likely due to the coarse spectral sampling of the  $H\alpha$  line in the models). At the extremes of the distribution ( $V - I < -0.1$  and  $V - I > 1$ ) the density of observed points decreases considerably. To determine the reference template there, we have reduced the box-car size to 10 points and averaged the running median obtained in this way with the theoretical models (thin solid line). The thick dot-dashed line in Figure 4 shows the best linear fit to the resulting average (which is extrapolated for  $V - I > 2$ ).

A total of 189 objects, indicated by large dots in Figure 4, have a  $V - H\alpha$  index exceeding that of the reference template at the same  $V - I$  colour by more than four times the uncertainty on their  $V - H\alpha$  values. These are the objects with a  $V - H\alpha$  excess at the  $4\sigma$  level and, as we shall see later, most of them are bona-fide PMS stars.

Since the contribution of the  $H\alpha$  line to the  $V$  magnitude is completely negligible, the magnitude  $\Delta H\alpha$  corresponding to the excess emission is simply:

$$\Delta H\alpha = (V - H\alpha)^{\text{obs}} - (V - H\alpha)^{\text{ref}} \quad (2)$$

where the superscript *obs* refers to the observations and *ref* to the reference template. Once  $\Delta H\alpha$  is determined in this way, the  $H\alpha$  emission line luminosity  $L(H\alpha)$  can be immediately obtained from the photometric zero point and absolute sensitivity of the instrumental set-up and from the distance to the sources. We have assumed a distance to the LMC and, more specifically, to SN 1987A of  $51.4 \pm 1.2$  kpc (Panagia et al. 1991, later updated in Panagia 1999), whereas the photometric properties of the instrument were taken from the WFPC2 Instrument Handbook (Heyer & Biretta 2004; namely inverse sensitivity  $\text{PHOTFLAM} = 1.461 \times 10^{-16}$  and

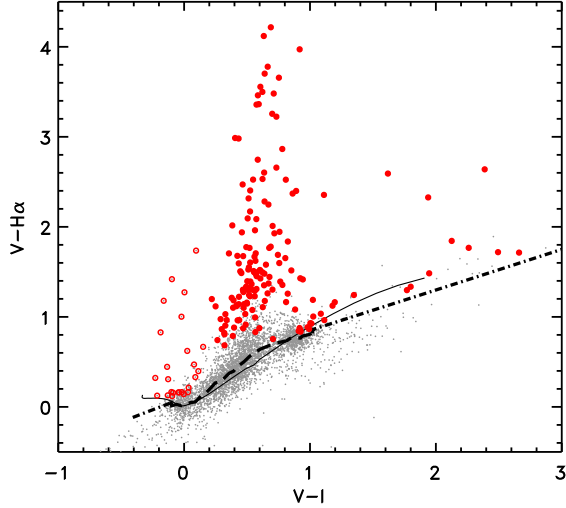


FIG. 4.— Colour-colour diagram of the selected 4156 stars in the field of SN 1987A. The dashed line represents the running median  $V-H\alpha$  colour, obtained with a box-car size of 100 points, whereas the thin solid line shows the model atmospheres of Bessell et al. (1998). A total of 189 objects with  $V-H\alpha$  excess larger than  $4\sigma$  are indicated with large dots.

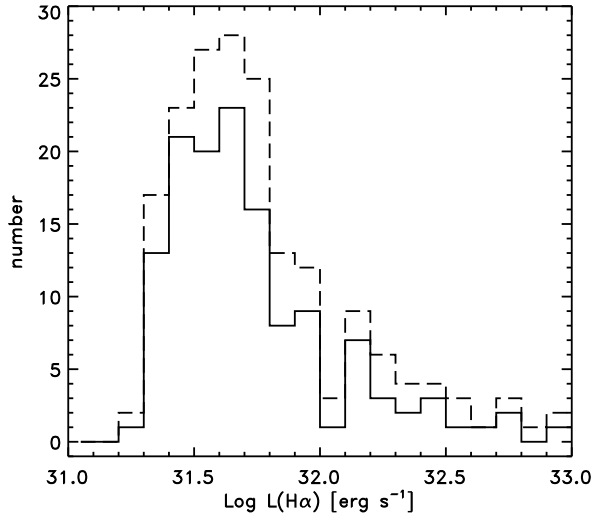


FIG. 5.— Histogram of the  $H\alpha$  luminosities of the 189 stars with  $H\alpha$  excess at the  $4\sigma$  level (dashed line) and of the 133 bona-fide PMS that also have an emission  $W_{\text{eq}}(H\alpha) > 10 \text{ \AA}$  and are not Ae/Be stars (solid line).

photometric zero-point  $ZP(\text{Vegmag}) = 17.564$ ). We derive a median value of the luminosity of the 189 objects with  $H\alpha$  excess of  $4 \times 10^{31} \text{ erg/s}$  or  $10^{-2} L_{\odot}$ . A histogram of the individual  $L(H\alpha)$  values is shown in Figure 5 (dashed line).

It should be noted that, because of the width of the  $H\alpha$  filter,  $\Delta H\alpha$  includes a small contribution due to [NII] emission features at  $6548 \text{ \AA}$  and  $6584 \text{ \AA}$ . Generally, their intensities do not exceed 1.2% and 3.5%, respectively, of the  $H\alpha$  line intensity, and in many instances the [NII] doublet lines are much weaker, i.e.  $< 0.1\%$  of the  $H\alpha$  line intensity (e.g. Edwards et al. 1987; Hartigan, Edwards & Ghandour 1995). These intensities should be even lower for PMS stars in the LMC because of the lower metallicity relative to the Milky Way. However, to take a conservative approach, we have simply adopted an

average value that is half of the maximum for Galactic T-Tauri stars and we give as uncertainty half of the measured range. We will therefore adopt average values of  $(1.8 \pm 1.8)\%$  and  $(0.6 \pm 0.6)\%$  relative to the  $H\alpha$  intensity, for the  $6584 \text{ \AA}$  and  $6548 \text{ \AA}$  [NII] lines, respectively (note that the uncertainties after the  $\pm$  sign here are meant to show the entire span of the range, not just the  $1\sigma$  value). Considering the width of the  $H\alpha$  filter of the WFPC2, only the  $6548 \text{ \AA}$  [NII] line contaminates the  $H\alpha$  measurements, whereas for measurements made with the  $H\alpha$  filter on board the ACS, both lines will be included (albeit only in part for the  $6548 \text{ \AA}$  line). Although the resulting corrections on the  $H\alpha$  intensity are quite small (namely 0.994 for the WFPC2 F656N filter and 0.979 for the ACS F658N filter, on average), they are systematic and it is therefore good practice to apply them in all cases.

Typically, the combined total uncertainty on our  $L(H\alpha)$  measurements is  $\sim 15\%$  and is completely dominated by the statistical uncertainty on the  $H\alpha$  photometry. The systematic uncertainty on the distance to the field of SN 1987A accounts for 5% (see Panagia 1999), whereas the typical uncertainty on the absolute sensitivity of the instrumental setup is of order 3%.

### 3.2. The $H\alpha$ equivalent width

If the stars defining the reference template had no  $H\alpha$  absorption features (we have established above that they do not have  $H\alpha$  in emission), their  $V-H\alpha$  index would correspond to that of the pure continuum and could then be used to derive the equivalent width of the  $H\alpha$  emission line,  $W_{\text{eq}}(H\alpha)$ . While this approximation might be valid for stars with a conspicuous  $H\alpha$  emission, it is clearly not applicable in general. It is, however, possible in all cases to derive the level of the  $H\alpha$  continuum by using properly validated models atmospheres.

As discussed above, the models of Bessell et al. (1998) reproduce quite reliably the observed broad-band colours (see e.g. Figure 2). This means that, even though the models might lack the resolution necessary to realistically reproduce spectral lines (hence the small discrepancy between the dashed line and the squares in Figure 3), the level of the continuum can be trusted. One can, therefore, fit the continuum in those models in a range containing the  $H\alpha$  line (e.g.  $6500-6620 \text{ \AA}$ ) and fold the resulting “ $H\alpha$ -less” model spectra through the instrumental set-up (e.g. with Synphot), so as to derive the magnitude of the sole continuum in the  $H\alpha$  band ( $H\alpha^c$ ) as a function of spectral type or effective temperature. We present in the Appendix the relationships between  $V$ ,  $I$  and  $H\alpha^c$  for several HST instruments and filters. The difference between the observed  $H\alpha$  magnitude and  $H\alpha^c$  provides a direct measure of  $W_{\text{eq}}(H\alpha)$ , as we explain below.

We recall that the equivalent width of a line is defined as:

$$W_{\text{eq}} = \int (1 - P_{\lambda}) d\lambda \quad (3)$$

where  $P_{\lambda}$  is the profile of the line, or the spectrum of the source divided by the intensity of the continuum, and the integration is extended over the spectral region corresponding to the line. If the line profile is very narrow when compared to the width of the filter, i.e. if the line falls completely within the filter bandpass as is typical of emission lines, then  $W_{\text{eq}}(H\alpha)$  is simply given by the relationship:

$$W_{\text{eq}}(H\alpha) = RW \times [1 - 10^{-0.4 \times (H\alpha - H\alpha^c)}] \quad (4)$$

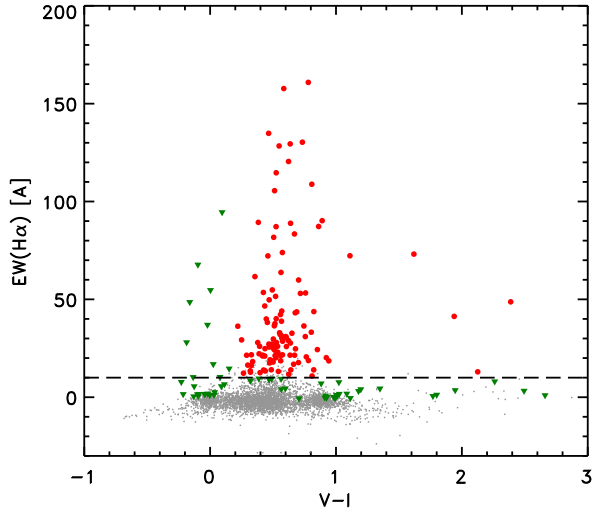


FIG. 6.— Equivalent width of the selected 4 156 stars in the field of SN 1987A, as a function of their  $V-I$  colour. Of the 189 stars with  $H\alpha$  excess at the  $4\sigma$  level (circles and triangles), a total of 164 have  $W_{\text{eq}}(H\alpha) > 10 \text{ \AA}$ . While objects bluer than  $V-I \simeq 0.2$  are probably Ae/Be stars, there are 133 redder stars with significant  $H\alpha$  excess (marked as circles) that we consider bona-fide low-mass PMS stars.

where  $RW$  is the rectangular width of the filter (similar in definition to the equivalent width of a line), which depends on the characteristics of the filter. Values of  $RW$  for the  $H\alpha$  bands of past and current HST instruments are given in the Appendix (Table 4). As in the case of  $L(H\alpha)$ , the statistical uncertainty on the equivalent width is dominated by the uncertainty on the  $H\alpha$  magnitude, typically of order 15% in our selection. Moreover, the value of  $W_{\text{eq}}(H\alpha)$  obtained in this way is also subject to some systematic uncertainties produced by the model atmospheres used to interpolate the level of the continuum, such as e.g. metallicity, surface gravity or spectral resolution, and should therefore be taken with caution. On the other hand, we show in the Appendix that the equivalent widths (in absorption) obtained by applying this method to the high-resolution model spectra of Munari et al. (2005) are in excellent agreement with those obtained via standard spectro-photometry (see Figure 18).

Similarly, the values of  $W_{\text{eq}}(H\alpha)$  that we obtain in the field of SN 1987A are fully consistent with those of young PMS stars. In Figure 6 we show the value of  $W_{\text{eq}}(H\alpha)$  as a function of  $V-I$  for the 4 156 selected stars. As mentioned earlier, there are 189 objects with a  $\Delta H\alpha$  excess above the  $4\sigma$  level and they are indicated as thick symbols (circles and triangles) in Figure 6. Since the equivalent width shown in Figure 6 is that of the pure emission component, the spectra of stars with small  $W_{\text{eq}}$ , say  $\lesssim 10 \text{ \AA}$ , actually show an  $H\alpha$  in absorption. For this reason, we conservatively ignore stars with measured  $W_{\text{eq}}(H\alpha) < 10 \text{ \AA}$ , since this value is about the largest absorption equivalent width expected for normal stars (see Figure 18 in the Appendix). A total of 164 objects satisfy this condition, but, in light of our conservative threshold, this must be considered as a lower-limit to the number of objects with genuine  $H\alpha$  excess.

Values of  $W_{\text{eq}}(H\alpha)$  for the sample range from  $10 \text{ \AA}$  to  $650 \text{ \AA}$ , with a median of  $19 \text{ \AA}$ . These values are in excellent agreement with those obtained by Panagia et al. (2000) from the  $R-H\alpha$  colour excess of the stars in this field and represent a refinement of those measurements, since these are based

on a more accurate determination of the level of the continuum. These equivalent widths are typical of PMS stars (e.g. Muzerolle, Hartmann & Calvet 1998) and about two orders of magnitude smaller than those expected for pure nebular emission (see discussion in Section 6). While objects bluer than  $V-I \simeq 0.2$  are probably Ae/Be stars, there are 133 redder stars with significant  $H\alpha$  excess (marked as circles in Figure 6) that are most likely bona-fide low-mass PMS stars of various ages, as we will show in the following sections. A histogram of their  $H\alpha$  luminosities is shown in Figure 5 (solid line).

#### 4. ACCRETION LUMINOSITY AND MASS ACCRETION RATE

It is generally accepted (see e.g. Hartmann et al. 1998) that the energy  $L_{\text{acc}}$  released by the magnetospheric accretion process goes towards ionising and heating the circumstellar gas. In this hypothesis, the bolometric accretion luminosity  $L_{\text{acc}}$  can be determined from a measurement of the *reradiated energy* and, in particular, via the measured  $H\alpha$  luminosity that is produced in the process.

In order to determine the exact relationship between  $L(H\alpha)$  and  $L_{\text{acc}}$ , we have used literature values of  $L_{\text{acc}}$  and  $L(H\alpha)$  measurements as recently summarized by Dahm (2008) for PMS stars in the Taurus–Auriga association. As pointed out by Dahm himself, there may be a serious problem in determining an empirical relationship between  $L_{\text{acc}}$  and  $L(H\alpha)$  measurements because the two quantities were determined from non-simultaneous observations. The intensity of the  $H\alpha$  line from PMS sequence stars is known to vary by about 20% on a time scale of a few hours and by as much as a factor of 2–3 in a few days (e.g. Fernandez et al. 1995; Smith et al. 1999; Alencar et al. 2001). For this reason, a relationship between  $L(H\alpha)$  and  $L_{\text{acc}}$  is necessarily rather uncertain, although a very clear trend can be seen in the  $L_{\text{acc}}$  vs.  $L(H\alpha)$  plot shown by Dahm (2008). His logarithmic best fit would provide a slope of  $1.18 \pm 0.26$  for such a relationship. On the other hand, theoretical models (e.g. Muzerolle, Calvet & Hartmann 1998) would predict logarithmic slopes of about unity for low accretion rates, hence for faint  $H\alpha$  luminosities, and shallower slopes for higher luminosities.

In the absence of compelling evidence in favour or against a steep slope, we will adopt a logarithmic slope of unity for the empirical  $L_{\text{acc}}$  vs.  $L(H\alpha)$  relationship, i.e. a constant ratio  $L_{\text{acc}}/L(H\alpha)$ , and determine the proportionality constant from an elementary fit of the data summarised by Dahm (2008). On this basis we obtain:

$$\log L_{\text{acc}} = (1.72 \pm 0.47) + \log L(H\alpha) \quad (5)$$

As anticipated, the resulting uncertainty on  $L_{\text{acc}}$  is rather large, as high as a factor of 3, but this is the best one can obtain with the available data sets. In view of the convenience and the feasibility of determining  $L_{\text{acc}}$  from  $L(H\alpha)$  for PMS outside our own Galaxy, it would be of paramount importance to obtain a proper calibration of the  $L_{\text{acc}}$  vs.  $L(H\alpha)$  relationship by making simultaneous spectral observations of PMS stars over a suitably wide wavelength baseline, i.e. covering at least the range  $3000\text{--}8000 \text{ \AA}$ , and possibly extending it to the near IR with measurements of Paschen and Brackett lines. High quality data of this type are already available for the Orion Nebula Cluster, collected by dedicated projects both from ground based observatories and with the HST (i.e. the Legacy Program on Orion; P.I. Massimo Robberto) and their analysis is in progress to provide a more accurate cal-

ibration of the  $L_{\text{acc}}$  vs.  $L(H\alpha)$  relationship (Da Rio et al., in preparation; Robberto et al., in preparation; Panagia et al., in preparation).

The median value of the accretion luminosity thus obtained for our sample of 133 PMS stars is  $\sim 0.57 L_{\odot}$ , in good agreement with the value of  $0.54 L_{\odot}$  derived from the U-band excess measured by Romaniello et al. (2004) for stars in the same field, especially considering that their selection of stars with excess emission is less stringent than our  $4\sigma$  level (we discuss this point in Section 7).

Once  $L_{\text{acc}}$  is known, the mass accretion rate follows from the free-fall equation that links the luminosity released in the impact of the accretion flow with the rate of mass accretion  $\dot{M}_{\text{acc}}$  according to the relationship:

$$L_{\text{acc}} \simeq \frac{GM_* \dot{M}_{\text{acc}}}{R_*} \left(1 - \frac{R_*}{R_{\text{in}}}\right) \quad (6)$$

where  $G$  is the gravitational constant,  $M_*$  and  $R_*$  the mass and photospheric radius of the star and  $R_{\text{in}}$  the inner radius of the accretion disc. The value of  $R_{\text{in}}$  is rather uncertain and depends on how exactly the accretion disc is coupled with the magnetic field of the star. Following Gullbring et al. (1998), we adopt  $R_{\text{in}} = 5R_*$  for all PMS objects.

As regards  $R_*$ , we derive it from the luminosity and effective temperature of the stars, which in turn come from the observed colour ( $V-I$ ) and magnitude ( $V$ ), properly corrected for interstellar extinction as provided by Romaniello (1998), Panagia et al. (2000) and Romaniello et al. (2002). The adopted distance to SN 1987A is 51.4 kpc (Panagia et al. 1991; Panagia 1999), as mentioned above. The stellar mass  $M_*$  was estimated by comparing the location of a star in the Hertzsprung–Russell (H–R) diagram with the PMS evolutionary tracks. As for the latter, we adopted those of Degl’Innocenti et al. (2008; see also Tognelli, Prada Moroni & Degl’Innocenti, in preparation), for metallicity  $Z = 0.007$  or about one third  $Z_{\odot}$ , as appropriate for the LMC (e.g. Hill, Andrievsky, & Spite 1995; Geha et al. 1998). These new PMS tracks were specifically computed with an updated version of the FRANEC evolutionary code (see Chieffi & Straniero 1989 and Degl’Innocenti et al. 2008 for details and Cignoni et al. 2009 for an application). However, in order to assess how differences in the evolutionary models affect our results, in Section 6.1 we also consider PMS tracks from other authors, namely those of D’Antona & Mazzitelli (1997) and Siess, Dufour & Forestini (2000).

Combining Equations 5 and 6, we can link the mass accretion rate  $\dot{M}_{\text{acc}}$ , in units of  $M_{\odot} \text{ yr}^{-1}$ , to  $L(H\alpha)$ :

$$\begin{aligned} \log \frac{\dot{M}_{\text{acc}}}{M_{\odot} \text{ yr}^{-1}} &= -7.39 + \log \frac{L_{\text{acc}}}{L_{\odot}} + \log \frac{R_*}{R_{\odot}} - \log \frac{M_*}{M_{\odot}} \quad (7) \\ &= (-5.67 \pm 0.47) + \log \frac{L(H\alpha)}{L_{\odot}} + \log \frac{R_*}{R_{\odot}} - \log \frac{M_*}{M_{\odot}} \end{aligned}$$

The distribution of mass accretion rates found in this way for the 133 PMS stars in our sample is shown in Figure 7. The median value of  $2.9 \times 10^{-8} M_{\odot} \text{ yr}^{-1}$  is in remarkably good agreement with the median rate of  $2.6 \times 10^{-8} M_{\odot} \text{ yr}^{-1}$  found by Romaniello et al. (2004) from the U-band excess.

The uncertainty on  $\dot{M}_{\text{acc}}$  is dominated by the approximate knowledge of the ratio of  $L_{\text{acc}}$  and  $L(H\alpha)$  in Equation 5. As explained above, empirical measurements and theoretical

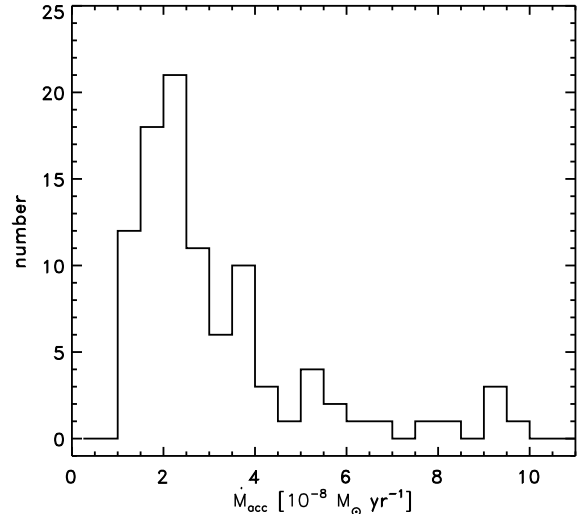


FIG. 7.— Distribution of the mass accretion rates of the 133 bona-fide PMS stars. Note that 9 objects with  $\dot{M}_{\text{acc}} > 10^{-7} M_{\odot} \text{ yr}^{-1}$  are not shown in the graph.

models suggest a value of  $L_{\text{acc}}/L(H\alpha) \simeq 52$  but with an uncertainty of a factor of three. Since the ratio, however, is the same for all stars, the comparison between different objects is not hampered by this uncertainty, as long as the statistical errors are small.

As for the other quantities in Equation 7, we discuss here the sources of statistical uncertainty, while systematic errors are addressed separately in Section 6. With our selection criteria, the typical uncertainty on  $L(H\alpha)$  is 15% and is dominated by random errors. The uncertainty on  $R_*$  is typically 7%, including a 5% systematic uncertainty on the distance modulus. As for the mass  $M_*$ , since it is determined by comparing the location of a star in the H–R diagram with evolutionary tracks, both systematic and statistical uncertainties are important. The uncertainty on the temperature is mostly statistical and of order 3%, while that on the luminosity is 7%, comprising both random errors (1% uncertainty on the bolometric correction and 3% on the photometry) and systematic effects (5% uncertainty on the distance modulus). When we interpolate through the PMS evolutionary tracks to estimate the mass, the uncertainties on  $T_{\text{eff}}$  and  $L$  imply an error of  $\sim 7\%$  on  $M_*$ . However, an even larger source of systematic uncertainty on  $M_*$  comes from the evolutionary tracks, as we explain in Section 6. In summary, the combined statistical uncertainty on  $\dot{M}_{\text{acc}}$  is 17%.

## 5. AGES OF PMS STARS

Having identified a population of bona-fide PMS stars, with well defined accretion luminosities and mass accretion rates, it is instructive to place them in the H–R diagram. We do so in Figure 8 where bona-fide PMS stars are marked as large dots, with a size proportional to their  $\dot{M}_{\text{acc}}$  value, according to the legend. Also shown in the figure are the theoretical isochrones from the FRANEC models of Degl’Innocenti et al. (2008) for  $Z = 0.007$  and ages as indicated (in units of Myr, from the stellar birth line; see Palla & Stahler 1993). The dashed line, corresponding to a 40 Myr isochrone, defines in practice the zero-age main sequence (MS).

It is noteworthy that the majority of PMS objects in Figure 8 are rather close to the MS and would have easily been



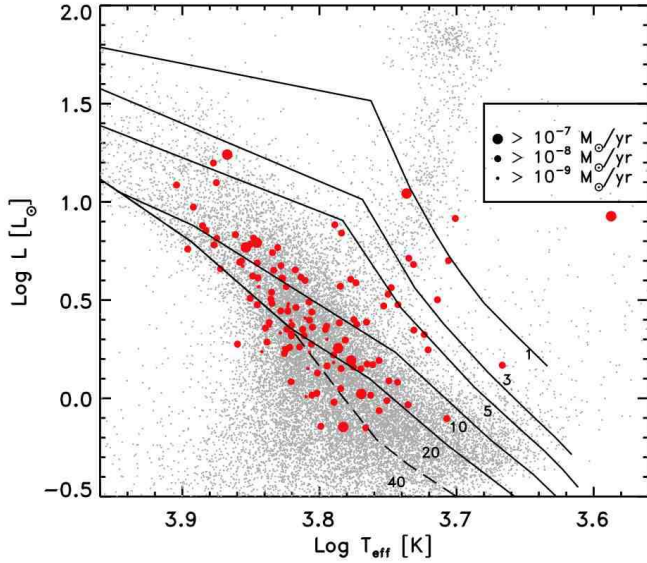


FIG. 8.— Location of the bona-fide PMS candidates in the H–R diagram, compared with the isochrones of Degl’Innocenti et al. (2008) for metallicity  $Z = 0.007$  (the ages, in Myr, are indicated next to each isochrone). The size of the symbols is proportional to the mass accretion rate  $\dot{M}_{\text{acc}}$  (see legend).

missed if no information on their  $H\alpha$  excess had been available. Indeed, it is customary to identify PMS stars in a colour–magnitude diagram by searching for objects located above and to the right of the MS, since this is where one would expect to find very young objects. This method was first used by Gilmozzi et al. (1994) to identify a population of PMS stars outside the Milky Way, namely in the LMC cluster NGC 1850. More recent applications of this method include e.g. those of Sirianni et al. (2000), Nota et al. (2006) and Gouliermis et al. (2006).

Unfortunately, this method of identification is not very reliable, since the existence of an age spread and the presence in the same field of a considerably older population, as well as unaccounted patchy absorption, all tend to fill up the parameter space between the MS and the birth line, thereby thwarting any attempts to identify PMS stars on the basis of their effective temperature and luminosity alone. In the specific case of the SN 1987A field studied here, Panagia et al. (2000) have shown that the age spread is remarkable, with several generations of young stars with ages between 1 and 150 Myr superposed on a much older field population (0.6–6 Gyr). In such circumstances, as Figure 8 shows, broad-band photometry alone would have not identified as such most of our bona-fide PMS stars.

In accordance with their proximity to the MS, the majority of bona-fide PMS stars turn out to be relatively old. The ages of individual objects were determined by interpolating between the isochrones in the H–R diagram. They range from 1 to  $\sim 50$  Myr, with a median age of 13.5 Myr, in very good agreement with the estimated age of both SN 1987A and its nearby Star 2 of  $\leq 13$  Myr (see Scuderi et al. 1996 and references therein). Panagia et al. (2000) find that about 35% of the stars younger than 100 Myr in this field have a typical age of 12 Myr, again consistent with the estimated age of the bona-fide PMS stars.

The relatively old age of our PMS stars might appear at odds with the rather large mass accretion rates that we obtain for that population, namely  $\sim 10^{-8} M_{\odot} \text{ yr}^{-1}$ . According to current models of viscous disc evolution (see Hart-

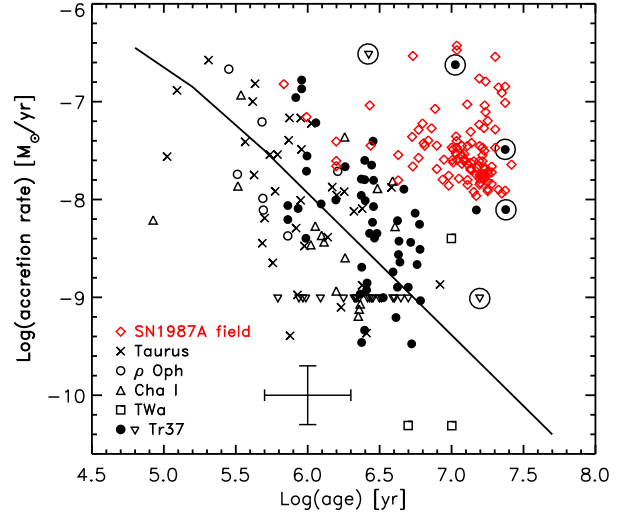


FIG. 9.— The mass accretion rate as a function of stellar age for our bona-fide PMS stars (diamonds) is compared here with that of a similar number of Galactic T Tauri stars (see legend) from the work of Sicilia-Aguilar et al. (2006), from whom all Galactic data-points are taken (the large cross indicates the uncertainties as quoted in that paper). The solid line shows the evolution for current models of viscous disc evolution from Hartmann et al. (1998). Our measurements are systematically higher than the models, but are in agreement with the  $\dot{M}_{\text{acc}}$  values of G type stars in the Galaxy (large circles).

mann et al. 1998; Muzerolle et al. 2000), the mass accretion rate of a  $\sim 14$  Myr old PMS population should be of order  $3 \times 10^{-10} M_{\odot} \text{ yr}^{-1}$ . Those models, shown in Figure 9 as a solid line, adequately reproduce the trend of decreasing  $\dot{M}_{\text{acc}}$  with stellar age observed for very low-mass Galactic T-Tauri stars (see e.g. Calvet et al. 2004), but under-predict our measurements (indicated by diamonds) by over an order of magnitude.

On the other hand, recent observations of PMS stars in the cluster Trumpler 37 by Sicilia-Aguilar et al. (2006), from whom the data-points in Figure 9 are taken, indicate that the value of  $\dot{M}_{\text{acc}}$  for  $\sim 10$ –20 Myr old G-type PMS stars (large circles) is considerably larger, indeed of order  $\sim 10^{-8} M_{\odot} \text{ yr}^{-1}$ , in excellent agreement with our results. With a median mass of  $1.2 M_{\odot}$  and a median  $V-I$  colour of 0.56, our bona-fide PMS stars are fully consistent with the G spectral type and suggest that stars of higher mass have a higher  $\dot{M}_{\text{acc}}$  value at all ages. As mentioned in the Introduction, Muzerolle et al. (2003; 2005), Natta et al. (2004; 2006) and Calvet et al. (2004) suggest a dependence of the type  $\dot{M}_{\text{acc}} \propto M^2$  from the analysis of a sample of low-mass and intermediate-mass T-Tauri stars, albeit with a large uncertainty on the index (see also Clarke & Pringle 2006). A similar trend is proposed by Sicilia-Aguilar et al. (2006), yet with even lower statistical significance due to the limited mass range covered by their observations. The range of masses that we cover here is also quite limited and does not allow us to address this issue in detail. We will, however, do so in a forthcoming paper (De Marchi et al. 2008, in preparation), where we compare the accretion rates in this field with those of a much younger and an order of magnitude more numerous population of PMS stars in the Small Magellanic Cloud. While in the SN 1987A field the detection limits imposed by the WFPC2 photometry do not allow us to reach stars with mass below  $\sim 0.9 M_{\odot}$ , in that paper, based on ACS observations, we will study stars down

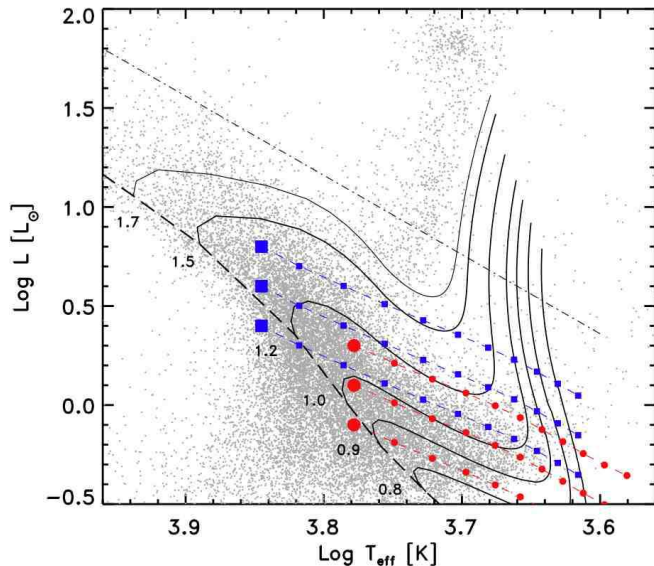


FIG. 10.— Simulated effects of a reddening increase on the mass determination via interpolation through the evolutionary tracks. The solid lines are the track of Siess et al. (2000) corresponding to the masses as indicated. Small circles and squares show the reddening displacement, from the unreddened locations (larger circles and squares), in increments of  $E(V-I) = 0.1$  according to the extinction law of Scuderi et al. (1996) for this field. The dot-dashed line indicates the line of constant radius, while the thick dashed line is the same 40 Myr isochrone as in Figure 8.

to  $\sim 0.4 M_{\odot}$ .

## 6. SYSTEMATIC ERRORS

The main sources of systematic uncertainty on the derived mass accretion rates are (i) discrepancies in the isochrones and evolutionary tracks, (ii) reddening, (iii)  $H\alpha$  emission generated by sources other than the accretion process, and (iv) the contribution of the nebular continuum to the colours of the stars. We discuss all these effects in this section.

### 6.1. Models of stellar evolution

As explained in Sections 4 and 5, the mass and age of PMS stars are determined by interpolation of their location in the H–R diagram, using model evolutionary tracks and isochrones as references. Apart for possible inaccuracies in the models input physics and errors in the interpolation, the largest source of systematic uncertainty on the derived mass and age comes from the use of models that might not properly describe the stellar population under study (e.g. because of the wrong metallicity) and from differences between models of various authors.

For instance, if we had used Siess et al.’s (2000) tracks for metallicity 1/2 solar in place of those for 1/3 solar, the masses of our PMS objects would be systematically higher by about 20%. For metallicity 1/2 solar, using the tracks of Siess et al. (2000) or those of D’Antona & Mazzitelli (1997) results in masses that agree to within a few percent. On the other hand, when it comes to the determination of the age, using D’Antona & Mazzitelli’s (1997) isochrones one would derive ages twice as young for stars colder than  $\sim 6500$  K, while for hotter stars ages would only be 20% lower.

In summary, systematic uncertainties of order 20% are to be expected for the mass and possibly higher for the age determination.

### 6.2. Reddening

Dust extinction systematically displaces stars in the H–R diagram towards lower luminosities and effective temperatures. This is shown graphically in Figure 10, for six model stars, three with  $T_{\text{eff}} = 6000$  K (large circles) and three with  $T_{\text{eff}} = 7000$  K (large squares). The effects of a reddening increase from  $E(V-I) = 0$  to  $E(V-I) = 1$  on the location of the stars in the H–R diagram is shown by the smaller symbols, corresponding to increments of  $E(V-I) = 0.1$ . We have adopted here the extinction law as measured specifically in the field of SN 1987A by Scuderi et al. (1996).

Since the reddening vector in the H–R plane is almost parallel to the lines of constant radius (as shown by the dot-dashed line for  $R = 10 R_{\odot}$ ), extinction affects only marginally the estimate of the stellar radius. However, at low temperatures the reddening vector crosses the evolutionary tracks (solid lines), thus leading to an underestimate of the stellar mass, if no extinction correction is applied. In turn, this will result in a systematically higher value of the  $R_*/M_*$  ratio and, therefore, in an overestimate of the mass accretion rate derived via Equation 6.

In order to better gauge the uncertainty on the value of  $R_*/M_*$  caused by unaccounted extinction, we have determined the mass and radius of each one of the artificially reddened model stars shown in Figure 10, in exactly the same way in which we did that for bona-fide PMS stars, and compared those with the known input values. The result is shown graphically in Figure 11, where, the relation between the derived and input  $R_*/M_*$  ratios is shown as a function of colour excess  $E(V-I)$ .

Regardless of the input parameters ( $L$ ,  $T_{\text{eff}}$  or  $R_*/M_*$ ), it appears that over the range explored here the derived  $R_*/M_*$  ratio increases slowly with colour excess (see dashed line that best fits the median values indicated by the crosses). In particular, underestimating the  $E(V-I)$  colour excess by  $\sim 0.4$  mag would lead to a 30% overestimate of  $R_*/M_*$  (and hence of  $\dot{M}_{\text{acc}}$ ). This appears unlikely, considering that the best estimate of the total extinction — including the Milky Way component — towards Star 2, one of the two bright close companions to SN 1987A, is  $E(V-I) = 0.21$  (Scuderi et al. 1996), with a  $1\sigma$  dispersion over the field of  $\sim 0.07$  (Romaniello 1998; Panagia et al. 2000). According to Zaritsky et al. (2004), the average reddening towards cool ( $5500 \text{ K} < T_{\text{eff}} < 6500 \text{ K}$ ) stars in the LMC is  $A_V = 0.43$ , thus implying  $E(V-I) \simeq E(B-V) \simeq 0.14$ . Therefore, for an average LMC star forming region, omitting the extinction correction would result in a 10% overestimate of the mass accretion rate. This error, albeit systematic, is smaller than most other systematic uncertainties and comparable to the measurement errors.

Nonetheless, we would like to stress here that the effects of patchy absorption can be more severe in regions of high extinction. Therefore, whenever possible, one should apply extinction corrections to each individual stars, as it was done for the photometric catalogue of Romaniello et al. (2002) that we use here.

### 6.3. $H\alpha$ emission not due to the accretion process

The underlying assumption in the determination of the mass accretion rate of PMS stars is that the gravitational energy  $L_{\text{acc}}$  released in the accretion process goes into heating of the gas at the boundary layer (see e.g. Hartmann et al. 1998). In this case, the luminosity of the  $H\alpha$  emission line can provide a measure of the accretion energy, because it acts as a natural

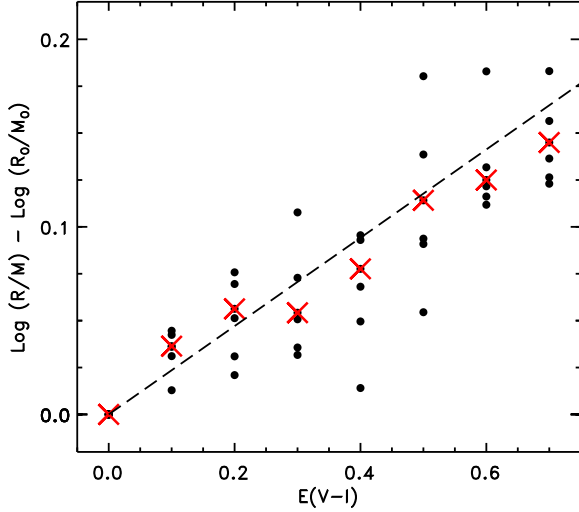


FIG. 11.— Overestimate of the  $R/M$  ratio as a function of  $E(V-I)$  when the extinction remains unaccounted. Thick dots represent the  $R/M$  ratios of the artificially reddened stars (see Figure 10) and the crosses their median values.

“detector” of the luminosity released in the accretion process.

Thus, the issue to address is whether the measured  $L(H\alpha)$  is produced only and entirely as a result of the energy released in the accretion process. Obviously, depending on the geometry and orientation of the circumstellar disc and on the specifics of the accretion process, some of the ionising energy could escape without effectively ionising the local gas. This would result in an underestimate of the true mass accretion rate for some stars, but this is true of any method that uses H emission lines as indicators of the accretion process and, therefore, it does not affect the comparison of our results with those of others (see Figure 9).

One possibility that we can readily exclude is that the  $H\alpha$  emission that we detect is due to chromospheric activity. The total chromospheric emission of a solar-type star on the sub-giant branch corresponds to a luminosity of about  $10^{-4} L_{\odot}$  (Ulmschneider 1979; Pasquini et al. 2000), i.e. two orders of magnitude less than what we measure.

On the other hand, we must also consider the possibility that  $H\alpha$  emission might occur in discrete H knots along the line of sight, in places unrelated with the PMS object. Furthermore, hot nearby massive stars may ionise the H gas in which PMS stars are immersed, eventually producing  $H\alpha$  emission when the gas recombines. Both these effects would result in an overestimate of  $\dot{M}_{\text{acc}}$ , but we show below that the probability of this happening is very small.

As for intervening  $H\alpha$  emission along the line of sight, it would have to arise in knots of ionised H, e.g. very compact HII regions, contained within our photometric apertures. However, if such knots exist, they should not project only against stars and, therefore, narrow-band images should reveal  $H\alpha$  emission where broad-band imaging shows no or very low signal (see Section 6.3). Since this is not observed, statistical arguments rule out this possibility as a significant source of the observed  $H\alpha$  excess emission.

While it is possible that some of the  $H\alpha$  emission that we detect is due to diffuse nebular emission in the HII region not powered by the accretion process, if the emission is extended and uniform over an area of at least  $0''.5$  radius around the star its contribution cancels out with the rest of the background

when we perform aperture photometry (using an aperture of  $0''.2$  radius for the object and an annulus of  $0''.3 - 0''.5$  for the background). The subtraction would not work if the emission were not uniform, as for example in the case of a filament that projects over the star but that does not cover completely the background annulus. However, we have visually inspected all objects with excess  $H\alpha$  emission and excluded the few cases where a spurious filament of this type could be seen (see Romaniello 1998; Panagia et al. 2000).

Another case in which the emission does not cancel out is when the gas ionised by an external source is associated to the star and completely contained within our photometric aperture. We recall here that the typical size of a circumstellar disc is of order 100 AU (e.g. Hartmann et al. 1998), or about 0.02 pixel at the distance of SN 1987A, and that the median  $L(H\alpha)$  that we measure for our PMS stars is  $4 \times 10^{31} \text{ erg s}^{-1}$ , or about  $10^{-2} L_{\odot}$  (see Figure 5). We can then calculate how close a PMS star should be to a hot, UV-bright star for the latter to flood the PMS circumstellar disc with enough ionising radiation to cause at least 10% of the  $H\alpha$  luminosity that we measure from that source.

Let  $r = 100 \text{ AU}$  be the external radius of the circumstellar disc and  $d$  the distance to an ionising star that illuminates the disc, assumed to have zero inclination (i.e. face on), so that  $\phi = r^2/(4d^2)$  is the solid angle subtended by the disc. Let  $\beta_2$  be the recombination coefficient to the first excited level in an optically thick H gas. If  $V$  is the volume of the gas and  $n_e$  and  $n_p$  are the electron and proton densities per unit volume, the global ionisation equilibrium equation (case B; see Baker & Menzel 1938) is then:

$$N_L \phi = \beta_2 n_e n_p V \quad (8)$$

where  $N_L$  is the rate of ionising photons produced by the external star. Denoting with  $\alpha_{3,2}$  the  $H\alpha$  emission coefficient for the same gas, the luminosity of the  $H\alpha$  recombination line can be written as:

$$L(H\alpha) = \alpha_{3,2} n_e n_p V \quad (9)$$

which allows us to express the luminosity of the  $H\alpha$  emission caused by the external star as a function of its ionising photon rate  $N_L$ :

$$L^{\text{ext}}(H\alpha) = \alpha_{3,2}/\beta_2 N_L \phi. \quad (10)$$

The minimum distance beyond which the contribution of the ionising star to the total  $H\alpha$  emission becomes negligible (i.e. 10% or less) is given by:

$$d_{\text{min}}^2 = \frac{r^2}{4} \frac{\alpha_{3,2}}{\beta_2} \frac{10 N_L}{L(H\alpha)}. \quad (11)$$

Table 1 gives the value of  $\phi$  for a typical  $H\alpha$  luminosity of  $10^{-2} L_{\odot}$ , as a function of the spectral type of the ionising star. Here we have used the compilation of Panagia (1973) for the appropriate stellar parameters. The table also provides the minimum distance  $d_{\text{min}}$  in pc and in arcsec (at the distance of SN 1987A) for a circumstellar disc of radius  $r = 100 \text{ AU}$ . We recall here that 1 arcsec corresponds to 10 WFPC2 pixels. The brightest star in the field studied here is an object with  $\log T_{\text{eff}} = 4.7$  and  $\log(L/L_{\odot}) = 5.8$ , with an implied mass of  $\sim 60 M_{\odot}$  and an age less than 1 Myr (see Panagia et al. 2000). The corresponding value of  $N_L$ , from Panagia (1973), is  $4 \times 10^{49} \text{ s}^{-1}$ , thus implying  $d_{\text{min}} = 0.95 \text{ pc}$  or 38 WFPC2

TABLE 1  
POSSIBLE EFFECTS OF NEARBY IONISING STARS

SpT	$T_{\text{eff}}$ (K)	$\log(L/L_{\odot})$	$\log N_L$ ( $\text{s}^{-1}$ )	$\phi$	$d_{\text{min}}$ (pc)	$d_{\text{min}}$ ( $''$ )
O4	50 000	6.11	49.93	3.42e-08	1.31	5.26
O6	42 000	5.40	49.08	2.43e-07	0.49	1.97
O7	36 500	4.81	48.62	6.93e-07	0.29	1.17
O9	34 500	4.66	48.08	2.43e-06	0.16	0.62
B0	30 900	4.40	47.36	1.27e-05	0.07	0.27
B1	22 600	3.72	45.29	1.50e-03	0.01	0.03

NOTE. — The values of  $\phi$  and  $d_{\text{min}}$  are given for a 100 AU circumstellar H disc with a temperature of 10 000 K. For gas temperatures of 5 000 K and 20 000 K the value of  $\phi$  is respectively higher and lower by 7.5 %, while  $d_{\text{min}}$  is 3.6 % larger and smaller, respectively.

pixel for a gas temperature of 10 000 K. A careful inspection of the images shows that none of our candidate bona-fide PMS stars falls closer to this star than  $d_{\text{min}}$ . The same applies to the second and third brightest stars in the field, respectively with  $\log T_{\text{eff}} = 4.7$ ,  $\log(L/L_{\odot}) = 5$  and  $\log T_{\text{eff}} = 4.67$ ,  $\log(L/L_{\odot}) = 4.75$ , as well as to all fainter objects.

It is convenient to calculate, for each PMS object, the total  $H\alpha$  luminosity  $L^{\text{ext}}(H\alpha)$  caused by all neighbouring ionising stars, expressed as:

$$L^{\text{ext}}(H\alpha) = \frac{r^2}{4} \frac{\alpha_{3,2}}{\beta_2} \sum_{i=1}^N \frac{(N_L)_i}{d_i^2} \quad (12)$$

where  $(N_L)_i$  is the ionising photon rate of star  $i$  and  $d_i$  is its distance from the PMS object being considered. Besides the three brightest stars mentioned above, we have included as potential sources of the detected  $H\alpha$  emission an additional 12 stars in the field with  $\log T_{\text{eff}} \geq 4.4$  and  $\log(L/L_{\odot}) \geq 4$ , as classified by Romaniello et al. (2002). We note that these estimates of  $L^{\text{ext}}(H\alpha)$  are firm upper limits because we are assuming that (i) all disks are *face-on* relative to the hot stars, and that (ii) the projected distances on the sky are indeed the actual distances from the hot stars. The values of  $L^{\text{ext}}(H\alpha)$  obtained in this way for the 133 bona-fide PMS stars span the range  $10^{-6} - 10^{-4} L_{\odot}$ , or typically three orders of magnitude less than the median PMS  $H\alpha$  luminosity, as shown by the histogram in Figure 12. We can, therefore, conclude that in this specific field the contribution of hot ionising stars to the measured excess  $H\alpha$  emission is negligible. We must stress, however, that the effect might be much more pronounced in younger star forming regions, such as the Orion Nebula or 30 Dor.

#### 6.4. Nebular continuum

Finally, consideration must be given to the role of the nebular continuum, i.e. radiation caused by bound-free and free-free transitions in the gas and unrelated to the stellar photosphere. If present, nebular continuum will add to the intrinsic continuum of the star, thereby affecting both the observed total level and the slope. This could ultimately alter the measured broad-band colours of the source, thereby thwarting our attempts to infer the level of the continuum in the  $H\alpha$  band from the observed  $V$  and  $I$  magnitudes. It is important to estimate the magnitude of this effect, as our method relies on the intrinsic  $V-I$  colour of a star to derive its  $\Delta H\alpha$  (see Equation 2).

Fortunately, the contribution of the nebular continuum appears to be insignificant. To prove this, we have assumed

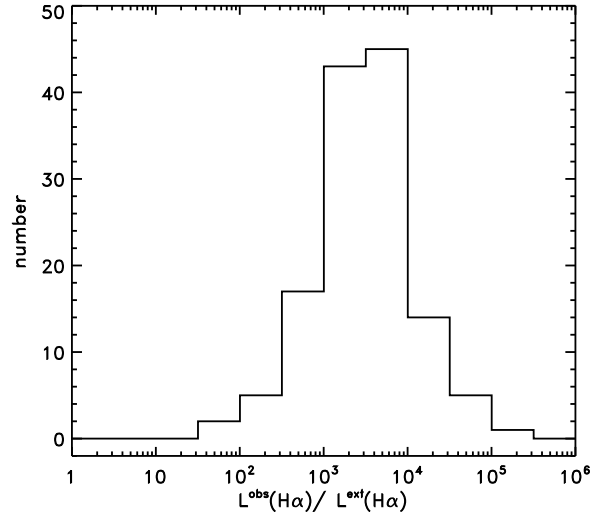


FIG. 12.— Histogram of the ratio of observed and external  $H\alpha$  luminosity for our bona-fide PMS stars. The observed  $H\alpha$  luminosity is typically three to four orders of magnitude larger than the contribution due to external sources.

TABLE 2  
NEBULAR EMISSION AND CONTINUUM OF FULLY IONISED H GAS

$T_{\text{el}}$	$F_{\nu}$	$F_{\lambda}$	$E(H\alpha)$	$W_{\text{eq}}(H\alpha)$
5 000 K	$10.28 \cdot 10^{-40}$	$7.16 \cdot 10^{-29}$	$6.71 \cdot 10^{-25}$	9378 Å
10 000 K	$7.56 \cdot 10^{-40}$	$5.26 \cdot 10^{-29}$	$3.56 \cdot 10^{-25}$	6763 Å
20 000 K	$5.51 \cdot 10^{-40}$	$3.83 \cdot 10^{-29}$	$1.83 \cdot 10^{-25}$	4764 Å

NOTE. —  $F_{\nu}$ ,  $F_{\lambda}$  and  $E(H\alpha)$  are given here in  $\text{erg cm}^3 \text{s}^{-1} \text{Hz}^{-1}$ , i.e. per unit volume ( $V$ ), unit electron density ( $n_e$ ) and unit proton density ( $n_p$ ). The luminosity can be derived by multiplying the values listed here by  $V n_e n_p$ .

a fully ionised gas of pure H, considering only bound-free and free-free transitions and ignoring the contribution to the continuum from two-photon emission (Spitzer & Greenstein 1951). Using Osterbrock's (1989, Chapter 4) tabulations, we find  $H\alpha$  line intensity and  $H\alpha$  continuum fluxes of the nebular gas as shown in Table 2, for gas electron temperatures in the range 5 000 K – 20 000 K. The purely nebular  $W_{\text{eq}}(H\alpha)$  ranges from 5 000 Å to 9 000 Å, or two orders of magnitude higher than what we measure for PMS objects. We can, therefore, safely conclude that the nebular contribution to the continuum is negligible (less than 1 %).

Furthermore, we find that for gas temperatures in the range 5 000 K – 10 000 K the  $V-I$  colour of the nebular continuum varies from 1.4 to 0.5, spanning a range typical of G–K type stars. Thus the effects of the nebular continuum on the  $V-I$  colour of PMS stars remains insignificant even for the objects with the highest  $W_{\text{eq}}(H\alpha)$  in our sample.

## 7. DISCUSSION AND CONCLUSIONS

We have developed and successfully tested a new self-consistent method to reliably identify all PMS objects actively undergoing mass accretion in a resolved stellar population, regardless of their age, without requiring spectroscopy. The method combines broad-band  $V$  and  $I$  photometry with narrow-band  $H\alpha$  imaging to: (1) identify all stars with excess  $H\alpha$  emission using as a reference template of the photospheric luminosity in the  $H\alpha$  band the average  $V-H\alpha$  colour of stars

with small photometric errors; (2) convert the excess  $H\alpha$  magnitude into  $H\alpha$  luminosity  $L(H\alpha)$  via the absolute photometric calibration of the  $H\alpha$  band; (3) convert, if desired, the excess  $H\alpha$  magnitude into the  $H\alpha$  emission equivalent width, using model spectra to fit the level of the continuum in the  $H\alpha$  band; (4) derive the accretion luminosity  $L_{\text{acc}}$  from  $L(H\alpha)$  using a relationship based on recent literature values; (5) obtain the mass accretion rate  $\dot{M}_{\text{acc}}$  from the free-fall equation that links it to  $L_{\text{acc}}$  via the stellar parameters (mass and radius), that we derive from the  $H$ - $R$  diagram using pre-main sequence tracks for the appropriate metallicity.

Since no spectroscopy of individual objects is needed, observations requiring just a few hours of exposure time can suffice to reveal hundreds of PMS stars simultaneously, determine their  $H\alpha$  luminosity with an uncertainty of less than 15% and derive their mass accretion rates with the same accuracy as allowed by conventional spectral line analysis.

As regards the  $H\alpha$  luminosity, the virtue of this new method is that it derives the reference luminosity of the stellar photosphere inside the specific  $H\alpha$  band simply from the average  $V-H\alpha$  colour of stars with the same  $V-I$  index (see Figure 4). This is possible because, at any given time, the majority of the stars in a stellar field have no excess  $H\alpha$  emission. Obviously, the average luminosity of the stellar photosphere in the  $H\alpha$  band reflects more or less pronounced  $H\alpha$  absorption features, depending on the spectral type of the objects, and precisely for this reason it defines the reference luminosity with respect to which any excess emission should be sought and measured. The uncertainty associated with the derived  $L(H\alpha)$  is dominated by statistical errors in the photometry and does not exceed 15% for our  $4\sigma$  selection (see Section 3.1). Note that this approach is also applicable to populations comprising mostly very young objects, such as the Orion Nebula, since excess  $H\alpha$  emission is found in only about one third of the PMS stars at any given time and, therefore, the majority of the very young objects will not have a conspicuous  $H\alpha$  emission, thus correctly defining the reference template (see Section 3.1).

In spite of the good accuracy on  $L(H\alpha)$ , deriving the mass accretion rate requires the use of a rather uncertain relationship linking  $L(H\alpha)$  to the accretion luminosity (see Section 4 and also Dahm 2008). The uncertainty on the relationship can have a systematic effect of up to a factor of 3 on the value of  $\dot{M}_{\text{acc}}$ . This is the unfortunate consequence of our incomplete understanding of the physics of the accretion process, plagued by the lack of direct measurements of the bolometric accretion luminosity  $L_{\text{acc}}$ , as well as by the paucity of simultaneous measurements of the hot continuum excess emission and of the emission line fluxes in  $H\alpha$  or other lines (e.g.  $\text{Pa}\beta$  and  $\text{Br}\gamma$ ). Although annoying, the systematic uncertainty of up to a factor of 3 on  $\dot{M}_{\text{acc}}$  is similar to that plaguing age determinations based on the comparison with theoretical isochrones, which can reach a factor of 2 (see Section 6.1).

On the other hand, these systematics affect in the same way all determinations of  $\dot{M}_{\text{acc}}$  that make use of emission lines diagnostics, including those based on a detailed study of the profile and intensity of the  $H\alpha$  line (e.g. Muzerolle et al. 1998b), since their calibration relies on the same measurements. For this reason, the relative values of  $\dot{M}_{\text{acc}}$  that we obtain are trustworthy and the comparison of our results with those obtained with other methods remains meaningful.

As discussed in Sections 3 and 4, as an application of our method, we have studied the field of SN 1987A, where we

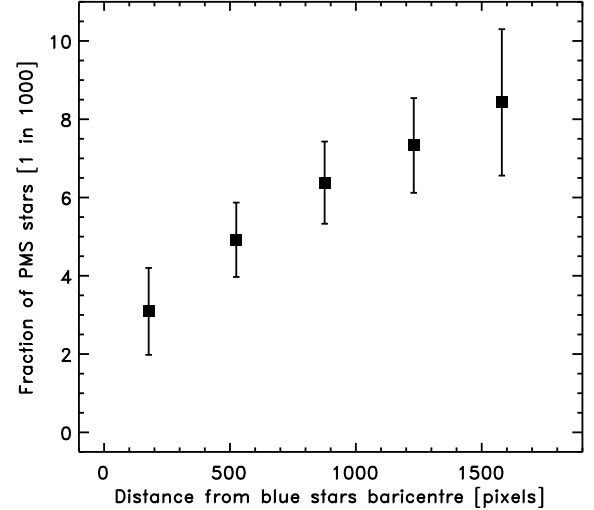


FIG. 13.— Fraction of PMS objects with respect to all stars, as a function of the distance (in units of WFPC2 pixel or  $0''.1$ ) from the baricentre of the ionising stars.

identify 133 bona-fide PMS stars, based on their large  $H\alpha$  excess. The median value of the mass accretion rate that we find for these stars, namely  $2.9 \times 10^{-8} M_{\odot} \text{ yr}^{-1}$ , is in very good agreement with the median value of  $2.4 \times 10^{-8} M_{\odot} \text{ yr}^{-1}$  found by Romaniello et al. (2004) from the analysis of the distribution of the  $(U-B)$  colour excess in the same field. While we have identified 133 bona-fide PMS stars with an  $H\alpha$  excess above the  $4\sigma$  level, Romaniello et al. conclude that 765 stars with an excess  $U$ -band luminosity larger than  $\sim 0.035 L_{\odot}$  could be bona-fide PMS candidates, albeit at the  $1.5\sigma$  level.

The approach followed by Romaniello et al. (2004) is statistical in nature and, while providing a solid estimate of the average mass accretion rate, it does not allow one to reliably identify individual PMS stars. Therefore, Romaniello et al. turned to the  $H\alpha$  excess emission (namely  $R-H\alpha$ ) as a more direct indicator of ongoing accretion and found a strong correlation between the  $U$ -band continuum excess and  $W_{\text{eq}}(H\alpha)$  for stars with  $U-B > 0.5$  and  $W_{\text{eq}}(H\alpha) > 3 \text{ \AA}$ . Not surprisingly, the more stringent threshold on the equivalent width adopted in the present study, i.e.  $W_{\text{eq}}(H\alpha) > 10 \text{ \AA}$ , results in a smaller number of identified bona-fide PMS stars, but also in a much smaller uncertainty. Indeed, the method that we present here is more direct than the one based on the  $U$ -band excess, since it does not require the use of model atmospheres to predict the level of the intrinsic photospheric continuum in the  $U$  band from the observed optical colours, and as such it results in a more reliable determination of the accretion luminosity.

Our method, therefore, makes it possible for the first time to carry out a quantitative and systematic study of the properties of a large number of PMS stars, including those in dense and/or distant star forming regions. This allows us to tackle some still open questions as to the evolution of both the stars and their discs. For instance, in the field of SN 1987A, we have studied how the mass accretion rate changes with time as our bona-fide PMS stars approach their main sequence. We find that  $\dot{M}_{\text{acc}}$  decreases more slowly with time than what is observed for low-mass T-Tauri stars in the Galaxy (see Section 5) and predicted by models of viscous disc evolution

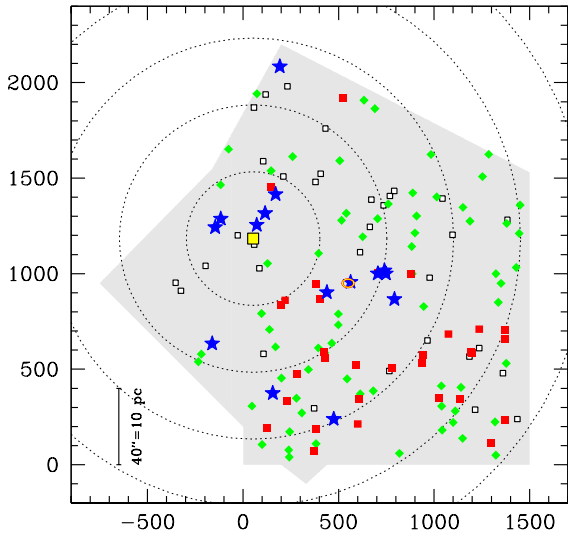


FIG. 14.— Map of the distribution of all bona-fide PMS objects with respect to the ionising stars (blue star symbols), whose baricentre is indicated by the large yellow square. Red squares correspond to stars with  $L(H\alpha) > 2 \times 10^{-2} L_{\odot}$ , white squares indicate objects with  $L(H\alpha) < 8 \times 10^{-3} L_{\odot}$ , and green diamonds are used for intermediate values. Note the paucity of PMS objects with high  $H\alpha$  luminosity near the baricentre of the ionising stars.

(Hartmann et al. 1998). However, our results are in excellent agreement with the (so far limited) measurements of the mass accretion rate of G type stars in the Milky Way (e.g. Sicilia-Aguilar et al. 2006), thus lending credit to the hypothesis that  $\dot{M}_{\text{acc}}$  might depend on the stellar mass.

Moreover, our method allows us to investigate whether and how the accretion process is affected by the chemical composition and density of the molecular clouds or by the proximity of hot, massive ionising stars. We will address the effects of metallicity in a forthcoming paper (De Marchi et al., in preparation) devoted to a comparison of star formation in the Small and Large Magellanic Clouds. As for the effect of hot massive stars, we have studied the distribution of the 133 bona-fide PMS objects with respect to the baricentre of the 15 hottest stars in the field, described in Section 6.3. We find a clear anti-correlation, shown in Figure 13, between the frequency of the identified PMS stars and their distance from the ionising objects (marked with blue star symbols in Figure 14). This effect is not seen for non-PMS objects of similar brightness, whose distribution is uniform over the whole field, confirming that the trend is not due to problems in detecting faint objects near the brightest stars. The trend remains the same whether the baricentre of the hot stars is computed using as weight their bolometric luminosity or their ionising flux. This anti-correlation is quite remarkable in several ways, as we discuss below.

In Figure 14 we show a schematic map of the distribution of all 133 PMS objects with respect to the 15 ionising stars. The baricentre of the ionising flux is shown by the large square and concentric annuli are drawn from it, in increments of  $35''$ . For reference, a red ellipse marks the position of SN 1987A. Symbols of different colours indicate PMS stars with different  $H\alpha$  luminosity, from red for  $L(H\alpha) > 2 \times 10^{-2} L_{\odot}$  to white for  $< 8 \times 10^{-3} L_{\odot}$ , with green diamonds corresponding to in-

termediate values. An inspection to Figure 14 immediately reveals two important facts: (i) there are very few PMS stars near the baricentre of the massive objects and (ii) their  $H\alpha$  luminosity is systematically lower than that of PMS stars farther away.

Panagia et al. (2000) had already pointed out that there is no overdensity of young PMS objects around hot massive stars in this field. This shows that low-mass and massive stars do not follow each other, suggesting that their formation mechanisms are separate and distinct. But what Figure 14 additionally shows is that there are very few PMS stars with strong  $H\alpha$  luminosity (red squares) around the young massive stars, with only 20 % of them within a 70 arcsec radius of the baricentre. Conversely, stars with low  $H\alpha$  luminosity (white squares) are distributed rather uniformly across the field.

With a median age of 13.5 Myr, most PMS objects are much older than the 1–2 Myr old hot stars and must belong to a previous generation. Thus, no spatial relationship (whether a correlation or anti-correlation) should be expected between the distribution of the two types of objects. On the other hand, while we cannot exclude that originally fewer PMS stars formed in the region now populated by young massive stars, there are indications that the local paucity of PMS objects is only apparent and caused by the presence of the hot young stars.

The fact that PMS objects near the youngest hot stars are both less numerous and fainter in  $H\alpha$  emission suggests that their circumstellar discs have been considerably eroded and made less efficient by enhanced photo-evaporation. We have shown earlier (see Section 6.3 and Figure 12) that the instantaneous contribution to the  $H\alpha$  luminosity from the ionising radiation of nearby massive stars is negligible. The results shown in Figure 14 confirms that this is the case. If it were not and the observed  $H\alpha$  luminosity were mostly due to fluorescence of the circumstellar discs under the effect of the ionising radiation of massive stars, the radial distribution should be opposite to the one observed, with brighter  $H\alpha$  luminosities for PMS stars closer to the baricentre of the youngest hot stars. Thus, if the apparent paucity of PMS objects in their vicinity is the result of photo-evaporation, the latter must be mostly due to the effects of non-ionising far ultraviolet (FUV) radiation. When integrated over the lifetime of massive stars ( $\sim 2$  Myr), their FUV radiation can be quite significant for the disruption of nearby circumstellar discs. In particular, this also means that there might be many more objects still in their PMS phase, close to the hot stars, but we have no way to identify them as such, since the photo-evaporation of their discs has stopped the accretion process.

Recent theoretical studies of the erosion of circumstellar discs via photo-evaporation due to external FUV radiation (e.g. Adams et al. 2004) or to the PMS star itself (e.g. Alexander, Clarke & Pringle 2006a; 2006b) suggest timescales of order 8–10 Myr for the complete dissolution of the discs. Although this is the right order of magnitude for the timescale of the process that we see, there are still some discrepancies. For instance, it is clear that if discs were to completely dissolve under the effect of their own central star within 5–10 Myr, as suggested by Alexander et al. (2006b), the majority of our PMS objects, with a median age of 13.5 Myr, should not show any sign of accretion. Similarly, with a typical age of 2 Myr, the hottest stars in our field would have not had time to deposit enough UV photons on to the PMS discs to seriously erode them, if the process is to take of order 10 Myr (Adams et al. 2004). While recently Clarke (2007) suggested that the

effect of nearby massive young stars may be stronger, leading to disc exhaustion timescales of order 2 Myr, her calculations apply to the immediate vicinity ( $< 1$  pc) of very massive stars, such as the O6 star  $\theta_1 C$  in Orion. The density of massive stars in the field of SN 1987A is much lower than that present in the Orion Nebula and the distances to our PMS objects typically an order of magnitude larger than those considered by Clarke (2007).

Nevertheless, while it is clear that the theory of disc photoevaporation does not yet capture all the details, we believe that it can greatly benefit from the observations presented here. In particular, it will be necessary to explain which mechanisms allow isolated circumstellar discs to feed their central PMS stars for well over 20 Myr, at least in a low-metallicity, low-density environment such as the field of the LMC. At the same time, the models should justify the quick ( $\lesssim 3$  Myr) demise of the PMS discs within a (projected) radius of  $\sim 10$  pc of a handful of late O stars. Extending our investigation, as we plan to do, to more and denser regions, such as NGC 1850 and 30 Dor in the Large Magellanic Cloud and NGC 346 and NGC 602 in the Small Magellanic Cloud, will offer increased statistics and a much wider variety of star formation environments.

We are very thankful to Pier Giorgio Prada Moroni and Scilla Degl’Innocenti for sharing with us their pre-main sequence evolutionary tracks ahead of publication and to Massimo Robberto for useful discussions. GDM is grateful to STScI and ESO for the hospitality, via their Science Visitor programmes, during the preparation of this paper. The research of NP was supported in part by NASA grant HST-GO-11547.06-A. We are also indebted to an anonymous referee for precious comments and suggestions that have helped us to improve the presentation of our work.

#### APPENDIX

Over the years, a large number of observations of stellar populations have been collected with the HST/WFPC2 and HST/ACS through the  $V$ -like filters F555W and F606W and the  $I$ -like filter F814W. We have therefore computed colour relationships between the magnitude in the  $R$ -like band F675W ( $m_{675}$ ) and the  $V-I$ -like colours  $m_{555} - m_{814}$  and  $m_{606} - m_{814}$ . To this aim, we have used both observed and theoretical stellar spectra, taken respectively from the Bruzual-Persson-Gunn-Stryker (BPGS) Spectrophotometry Atlas (see Gunn & Stryker 1983) and from the stellar atmosphere models of Bessell et al. (1998).

The BPGS atlas contains nearby bright dwarfs and giants of near-solar metallicity, whereas from the library of Bessell et al. (1998) we have selected specifically those models with metallicity index  $[M/H] = -0.5$ , as appropriate for the LMC (Dufour 1984), surface gravity  $g = 4.5$  and effective temperatures in the range  $3\,500 \text{ K} \leq T_{\text{eff}} \leq 40\,000 \text{ K}$ . Using the standard HST synthetic photometry package Synphot (Laidler et al. 2008), we have folded these spectra through the instrumental response of the WFPC2, the ACS/WFC, the ACS/HRC and the WFC3/UVIS cameras, in order to obtain the expected magnitudes in the bands listed above. For comparison with ground-based photometry, we have also calculated the expected magnitudes through the Johnson-Cousin  $V, R$  and  $I$  bands.

We show in Figure 15, for the WFPC2 filter system, the predicted  $m_{555} - m_{675}$  colour as a function of  $m_{555} - m_{814}$  for

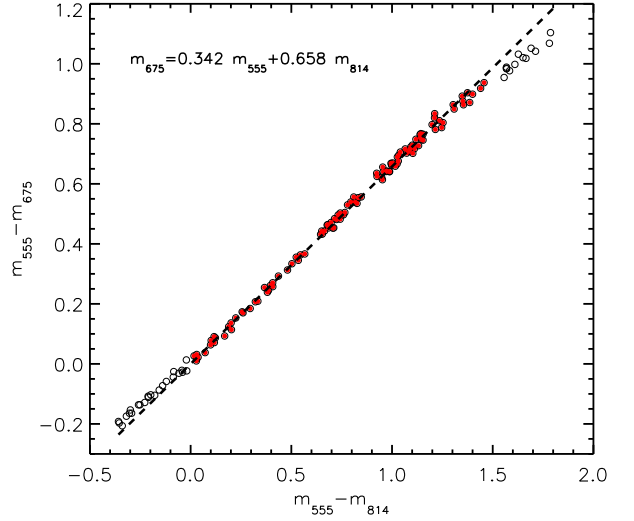


FIG. 15.— Relationship between the  $m_{555} - m_{675}$  and  $m_{555} - m_{814}$  colours of the WFPC2 filter system based on all the observed spectra in the BPGS atlas, with solar metallicity. The range over which the least square fit is carried out is indicated by filled circles.

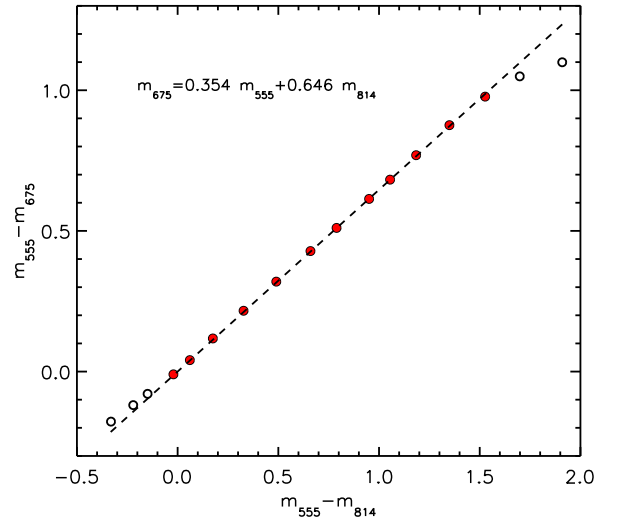


FIG. 16.— Relationship between the  $m_{555} - m_{675}$  and  $m_{555} - m_{814}$  colours of the WFPC2 filter system based on model spectra of Bessell et al. (1998) for metallicity  $[M/H] = -0.5$ . The range over which the least square fit is carried out ( $4000 \text{ K} < T_{\text{eff}} < 10000 \text{ K}$ ) is indicated by filled circles.

all the stars in the BPGS atlas. The distribution is remarkably linear and the dashed line represents the best fit in the colour range  $0 < m_{555} - m_{814} < 1.5$  (filled symbols), corresponding to the relationship  $m_{675} = 0.34 \times m_{555} + 0.66 \times m_{814}$ . The colour-colour diagram in the same bands based on the models of Bessell et al. (1998) is shown in Figure 16 and the relationship is practically indistinguishable, namely  $m_{675} = 0.35 \times m_{555} + 0.65 \times m_{814}$ . In this case, the dashed line shows the least-square fit to stars in the range  $4000 \text{ K} \leq T_{\text{eff}} \leq 10000 \text{ K}$ , marked by the filled symbols. As already noted in Section 2, it appears that neither the luminosity class nor the metallicity has a noticeable impact on the colour relationship in these bands.

This is also the case when we consider the  $m_{606} - m_{814}$  colour, for which the relationship with  $m_{675}$  is given in Ta-

TABLE 3  
PREDICTED COLOUR RELATIONS BETWEEN  $R$  OR  $H\alpha^c$  AND  $V-I$  FOR VARIOUS PHOTOMETRIC SYSTEMS.

System	Band	BPGS, $[M/H] = 0$	Bessell et al., $[M/H] = -0.5$	Bessell et al., $[M/H] = -1$
WFPC2	$m_{675}$	$0.342 \times m_{555} + 0.658 \times m_{814}$	$0.354 \times m_{555} + 0.646 \times m_{814}$	$0.353 \times m_{555} + 0.647 \times m_{814}$
	$m_{675}^c$	$0.510 \times m_{606} + 0.490 \times m_{814}$	$0.510 \times m_{606} + 0.490 \times m_{814}$	$0.508 \times m_{606} + 0.492 \times m_{814}$
	$m_{656}^c$		$0.409 \times m_{555} + 0.591 \times m_{814} - 0.351$	$0.411 \times m_{555} + 0.589 \times m_{814} - 0.350$
	$m_{656}^c$		$0.593 \times m_{606} + 0.407 \times m_{814} - 0.353$	$0.595 \times m_{606} + 0.405 \times m_{814} - 0.351$
ACS/ WFC	$m_{625}$	$0.496 \times m_{555} + 0.504 \times m_{814}$	$0.499 \times m_{555} + 0.501 \times m_{814}$	$0.503 \times m_{555} + 0.497 \times m_{814}$
	$m_{625}^c$	$0.708 \times m_{606} + 0.292 \times m_{814}$	$0.703 \times m_{606} + 0.297 \times m_{814}$	$0.708 \times m_{606} + 0.292 \times m_{814}$
	$m_{658}^c$		$0.381 \times m_{555} + 0.619 \times m_{814} - 0.156$	$0.386 \times m_{555} + 0.614 \times m_{814} - 0.158$
	$m_{658}^c$		$0.546 \times m_{606} + 0.454 \times m_{814} - 0.160$	$0.552 \times m_{606} + 0.448 \times m_{814} - 0.164$
ACS/ HRC	$m_{625}$	$0.506 \times m_{555} + 0.494 \times m_{814}$	$0.502 \times m_{555} + 0.498 \times m_{814}$	$0.511 \times m_{555} + 0.489 \times m_{814}$
	$m_{625}^c$	$0.707 \times m_{606} + 0.293 \times m_{814}$	$0.697 \times m_{606} + 0.303 \times m_{814}$	$0.704 \times m_{606} + 0.296 \times m_{814}$
	$m_{658}^c$		$0.385 \times m_{555} + 0.615 \times m_{814} - 0.160$	$0.390 \times m_{555} + 0.610 \times m_{814} - 0.160$
	$m_{658}^c$		$0.542 \times m_{606} + 0.458 \times m_{814} - 0.166$	$0.544 \times m_{606} + 0.456 \times m_{814} - 0.165$
WFC3/ UVIS	$m_{625}$	$0.504 \times m_{555} + 0.496 \times m_{814}$	$0.510 \times m_{555} + 0.490 \times m_{814}$	$0.517 \times m_{555} + 0.483 \times m_{814}$
	$m_{625}^c$	$0.742 \times m_{606} + 0.258 \times m_{814}$	$0.734 \times m_{606} + 0.266 \times m_{814}$	$0.741 \times m_{606} + 0.259 \times m_{814}$
	$m_{656}^c$		$0.387 \times m_{555} + 0.613 \times m_{814} - 0.405$	$0.389 \times m_{555} + 0.611 \times m_{814} - 0.408$
	$m_{656}^c$		$0.558 \times m_{606} + 0.442 \times m_{814} - 0.406$	$0.560 \times m_{606} + 0.440 \times m_{814} - 0.409$
Johnson- Cousin	$R$	$0.451 \times V + 0.549 \times I$	$0.465 \times V + 0.535 \times I$	$0.473 \times V + 0.527 \times I$

NOTE. — The typical  $1\sigma$  uncertainty on the slope of the regression fit is 0.003.

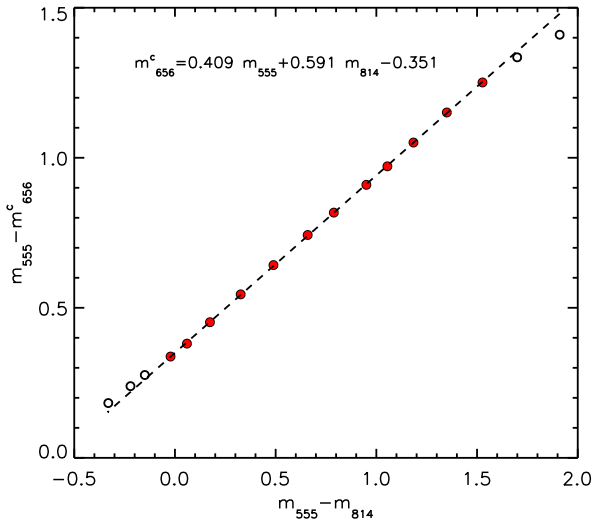


FIG. 17.— Relationship between the  $m_{555} - m_{656}^c$  and  $m_{555} - m_{814}$  colours of the WFPC2 filter system based on model spectra of Bessell et al. (1998), for metallicity  $[M/H] = -0.5$ , in which all spectral features in the range  $6500 - 6620 \text{ \AA}$  have been replaced by the continuum. The range over which the least square fit is carried out ( $4000 \text{ K} < T_{\text{eff}} < 10000 \text{ K}$ ) is indicated by filled circles.

ble3. In the same table we also list the results for the ACS/WFC, ACS/HRC and WFC3/UVIS cameras, as well as those for the standard Johnson–Cousin system normally used from the ground (note that the  $R$  and  $I$  bands in this system do not coincide with the  $R$  and  $I$  bands of Johnson’s original system, as mentioned in Section 2). As expected, the coefficients in the colour relationship vary considerably with the band, and differences exist also between the same band on various HST cameras (or, at least, bands with the same name).

As briefly discussed in Section 3, the magnitude corresponding to the level of the continuum in the  $H\alpha$  band can be derived by means of properly validated model atmospheres, such as those of Bessell et al. (1998) that we have shown to reproduce quite accurately the observed broad-band colours (see Figure 2). This means that, even though the models might lack the spectral resolution necessary to realistically repro-

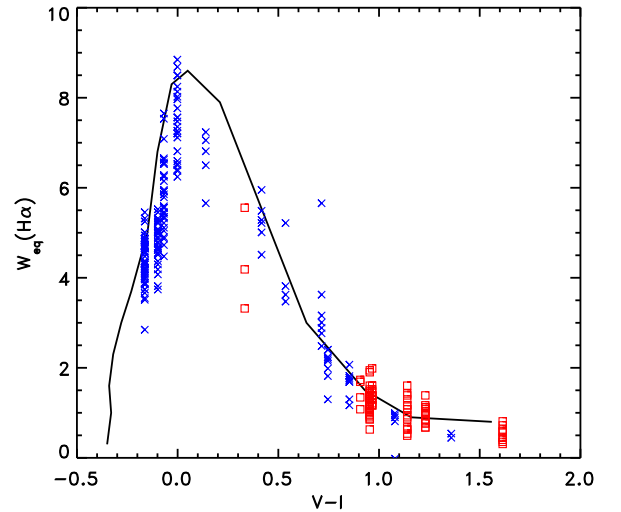


FIG. 18.— Comparison between the  $H\alpha$  absorption equivalent widths in the catalogue of Ducati (1981; crosses indicate dwarfs, squares are for giants) and those derived by applying Equation 4 to the spectral models of Munari et al. (2005) for solar metallicity (solid line).

duce spectral lines (hence the small discrepancy between the dashed lines and the squares in Figure 2), the level of the continuum can be trusted. We have, therefore, fitted the continuum in the Bessell et al. (1998) spectra over the range  $6500 - 6620 \text{ \AA}$  and have replaced the actual spectrum in that range with the interpolated continuum. Finally, we have used Synphot to fold the model spectra, modified in this way, through the instrumental set-up and derive in this way the continuum  $H\alpha$  magnitudes ( $H\alpha^c$ ) for the various  $H\alpha$  filters on-board the HST, as a function of the spectral type or  $T_{\text{eff}}$  of the star.

With this information it is now possible to build colour–colour diagrams like those of Figure 15 and 16, and look for a colour relationship between  $H\alpha^c$  and  $V-I$ . In Figure 17 we show the specific case of the WFPC2. The  $m_{555} - m_{656}^c$  colour varies very smoothly and very slowly with the effective temperature and is a remarkably linear function of the  $m_{555} - m_{814}$  colour over the whole range, and particularly for



TABLE 4  
RECTANGULAR WIDTH AND REFERENCE WAVELENGTH OF PAST AND  
PRESENT H $\alpha$  FILTERS INSTALLED ON BOARD THE HST.

Instrument	Filter	RW [ $\text{\AA}$ ]	$\lambda_{\text{ref}}$
WFPC2	F656N	28.35	6563.8
ACS/WFC	F658N	74.96	6584.3
ACS/HRC	F658N	74.96	6583.9
WFC3	F656N	17.68	6561.4
	F658N	27.61	6585.0

stars with  $4000 \text{ K} < T_{\text{eff}} < 10000 \text{ K}$  (filled circles) with which we are mostly concerned in this work. Similar relationships exist for other bands and photometric systems and they are given in Table 3. We note that the constant 0.351 in the colour relationship accounts for the conspicuous H $\alpha$  absorption line in the spectrum of Vega, which defines the standard for the VEGAMAG magnitude system.

As indicated in Section 3, the difference between the observed H $\alpha$  magnitude and  $H\alpha^c$  can be converted to the equivalent width  $E_{\text{eq}}(H\alpha)$  by means of Equation 4. To prove this, we have applied Equation 4 to the model atmospheres of Munari et al. (2005), which provide spectra with a resolving power of 11500 and a  $1 \text{ \AA}$  sampling, and compared the results to literature measurements of H $\alpha$  equivalent widths (in absorption).

Ducati (1981) compiled an extensive homogeneous catalogue of H $\alpha$  line measurements, from photographic and photoelectric techniques, for about 2300 stars. We have converted Ducati's index  $\alpha$  to  $W_{\text{eq}}(H\alpha)$  following the calibration provided by Strauss & Ducati (1981) and Cester et al. (1977). The values of  $W_{\text{eq}}(H\alpha)$  obtained in this way are shown in Figure 18, where crosses correspond to dwarfs and boxes to giants. Ducati's (1981) stars are classified according to their spectral type, which we have converted to  $V-I$  following Bessell (1990).

As for the application of Equation 4 to the models of Munari et al. (2005), this was done for model spectra with  $4000 < T_{\text{eff}}/\text{K} < 40000$ ,  $\log g = 4.5$  and solar metallicity and for the WFPC2 photometric system, namely F555W for V, F814W for I and F656N for H $\alpha$ . It should be noted that, for stars with broad H $\alpha$  lines (around spectral type A), the equivalent width determined in this way is systematically smaller than the true one, since part of the line wings fall outside of the H $\alpha$  filter. However, the measurements of Ducati (1981) are subject to exactly the same effect, since they were derived in a similar fashion and with a H $\alpha$  filter of comparable effective width. The value of  $W_{\text{eq}}(H\alpha)$  obtained in this way is shown in Figure 18 (solid line), as a function of  $V-I$ . The agreement with the observations is very satisfactory.

## REFERENCES

- Adams, F., Hollenbach, D., Laughlin, G., Gorti, U. 2004, *ApJ*, 611, 360  
Alencar, S., Johns-Krull, C., Basri, G. 2001, *AJ*, 122, 3335  
Alexander, R. D., Clarke, C. J., Pringle, J. E. 2006a, *MNRAS*, 369, 216  
Alexander, R. D., Clarke, C. J., Pringle, J. E. 2006b, *MNRAS*, 369, 229  
Appenzeller, I., Mundt, R. 1989, *A&ARv*, 1, 291  
Baker, J., Menzel, D. 1938, *ApJ*, 88, 52  
Bertout, C. 1989, *ARA&A*, 27, 351  
Bessell, M. 1990, *A&AS*, 83, 357  
Bessell, M., Castelli, F., Plez, B. 1998, *A&A*, 333, 231  
Calvet, N., Hartmann, L., Strom, E. 2000, in "Protostars and Planets", eds V. Mannings, A. Boss, S. Russell (Tucson: University of Arizona Press), 377  
Calvet, N., Muzerolle, J., Briceño, C., Hernandez, J., Hartmann, L., Saucedo, J. L., Gordon, K. D. 2004, *AJ*, 128, 1294  
Cester, B., Giuricin, G., Mardirossian, F., Pucillo, M., Castelli, F., Flora, U. 1977, *A&AS*, 30, 1  
Chieffi, A., Straniero, O. 1989, *ApJS*, 71, 47  
Cignoni, M., Sabbi, E., Nota, A., Tosi, M., Degl'Innocenti, S., Prada Moroni, P.G., Angeretti, L., Carlson, L.R., Gallagher, J., Meixner, M., Sirianni, M., Smith, L. 2009, *AJ*, 137, 3668  
Clarke, C. J. 2007, *MNRAS*, 376, 1350  
Clarke, C., Pringle, J. 2006, *MNRAS*, 370, L10  
Dahm, S. 2008, *AJ*, 136, 521  
D'Antona, F., Mazzitelli, I. 1997, *MmSAI*, 68, 807  
Degl'Innocenti, S., Prada Moroni, P.G., Marconi, M., Ruoppo, A. 2008, *Ap&SS*, 316, 25  
Drew, J., et al. 2005, *MNRAS*, 362, 753  
Ducati, J. 1981, *A&AS*, 45, 119  
Edwards, S., Cabrit, S., Strom, S., Heyer, I., Strom, K., Anderson, E. 1987, *ApJ*, 321, 473  
Fernandez, M., Ortiz, E., Eiroa, C., Miranda, L. 1995, *A&AS*, 114, 439  
Geha, M. et al. 1998, *AJ*, 115, 1045  
Gilmozzi, R., Kinney, E., Ewald, S., Panagia, N., Romaniello, M. 1994, *ApJ*, 435, L43  
Gouliermis, D. A., Henning, T., Brandner, W., Dolphin, A. E., Rosa, M., Brandl, B. 2007, *ApJ*, 665, L27  
Gullbring, E., Hartmann, L., Briceño, C., Calvet, N. 1998, *ApJ*, 492, 323  
Gunn, J., Stryker, L. 1983, *ApJS*, 52, 121  
Hartigan, P., Edwards, S., Ghandour, L. 1995, *ApJ*, 452, 736  
Hartmann, L., Calvet, P., Gullbring, E., D'Alessio, P. 1998, *ApJ*, 495, 385  
Herbig, G. 1957, *ApJ*, 125, 654  
Heyer, I., Biretta, J. 2004, "WFPC2 Instrument Handbook", (Baltimore: STScI)  
Hill, V., Andrievsky, S., Spite, M. 1995, *A&A*, 293, 347  
Horne, K. 1988, in "New Directions in Spectrophotometry", eds, A. Davis Philip, D. Hayes, S. Adelman (Schenectady: Davis Press), 145  
Hunter, D., Shaya, E., Holtzman, J., Light, R., O'Neil, E., Lynds, R. 1995, *ApJ*, 448, 179  
Johnson, H. L. 1966, *ARA&A*, 4, 193  
Königl, A. 1991, *ApJ*, 370, L39  
Koorneef, J., Bohlin, R., Buser, R., Horne, K., Turnshek, D. 1986, in "Highlights of astronomy", Volume 7, (Dordrecht: Reidel), 833  
Kohoutek, L., Wehmeyer, R. 1999, *A&AS*, 134, 255  
Laidler, V. et al. 2008, "Synphot Data User's Guide" (Baltimore: STScI)  
Lynden-Bell, D., Pringle, J. 1974, *MNRAS*, 168, 603  
Munari, U., Sordo, R., Castelli, F., Zwitter, T. 2005, *A&A*, 442, 1127  
Muzerolle, J., Hartmann, L., Calvet, N., 1998a, *AJ*, 116, 455  
Muzerolle, J., Calvet, N., Hartmann, L., 1998b, *ApJ*, 492, 743  
Muzerolle, J., Calvet, N., Briceño, C., Hartmann, L., Hillenbrand, L. 2000, *ApJ*, 535, L47  
Muzerolle, J., Hillenbrand, L., Calvet, N., Briceño, C., Hartmann, L., 2003, *ApJ*, 592, 266  
Muzerolle, J., Luhman, K., Briceño, C., Hartmann, L., Calvet, N. 2005, *ApJ*, 625, 906  
Natta, A., Testi, L., Muzerolle, J., Randich, S., et al. 2004, *A&A*, 424, 603  
Natta, A., Testi, L., Randich, S. 2006, *A&A*, 452, 245  
Nota, A., Sirianni, M., Sabbi, E., Tosi, M., Clampin, M., Gallagher, J., Meixner, M., Oey, M. S., Pasquali, A., Smith, L. J., Walterbos, R., Mack, J. 2006, *ApJ*, 640, L29  
Osterbrock, D. 1989, "Astrophysics of gaseous nebulae and active galactic nuclei", (Mill Valley: University Science Books)  
Padgett, D. 1996, *ApJ*, 471, 847  
Palla, F., Stahler, S. 1993, *ApJ*, 418, 414  
Panagia, N. 1973, *AJ*, 78, 929  
Panagia, N. 1999, in "New Views of the Magellanic Clouds", IAU Symp. 190, eds. Y.-H. Chu, N. Suntzeff, J. Hesser, D. Bohlender (San Francisco: ASP), 549  
Panagia, N., Gilmozzi, R., Macchetto, F., Adorf, H.-M., Kirshner, R. P. 1991, *ApJ*, 380, L23  
Panagia, N., Romaniello, M., Scuderi, S., Kirshner, R. 2000, *ApJ*, 539, 197  
Parker, Q., et al. 2005, *MNRAS*, 362, 689  
Pasquini, L., de Medeiros, J., Girardi, L. 2000, *A&A*, 361, 1011  
Romaniello, M. 1998, PhD thesis, Scuola Normale Superiore, Pisa, Italy  
Romaniello, M., Panagia, N., Scuderi, S., Kirshner, R. 2002, *AJ*, 123, 915  
Romaniello, M., Robberto, M., Panagia, N. 2004, *ApJ*, 608, 220  
Romaniello, M., Scuderi, S., Panagia, N., Salerno, R. M., Blanco, C. 2006, *A&A*, 446, 955

- Scuderi, S., Panagia, N., Gilmozzi, R., Challis, P., Kirshner, R. 1996, ApJ, 465, 956
- Sicilia-Aguilar, A., Hartmann, L., Hernandez, J., Briceño, C., Calvet, N. 2005, AJ, 130, 188
- Sicilia-Aguilar, A., Hartmann, L., Furesz, G., Henning, T., Dullemond, C., Brandner, W. 2006, AJ, 132, 2135
- Siess, L., Dufour, E., Forestini, M. 2000, A&A, 358, 593
- Sirianni, M., Jee, M., Benítez, N., Blakeslee, J., Martel, A., Meurer, G., Clampin, M., De Marchi, G., Ford, H. C., Gilliland, R., Hartig, G., Illingworth, G., Mack, J., McCann, W. 2005, PASP, 117, 1049
- Sirianni, M., Nota, A., Leitherer, C., De Marchi, G., Clampin, M. 2000, ApJ, 533, 203
- Shu, F., Najita, J., Ruden, S., Lizano, S. 1994, ApJ, 429, 727
- Smith, K., Lewis, G., Bonnell, I., Bunclark, P., Emerson, J. 1999, MNRAS, 304, 367
- Spitzer, L., Greenstein, J. 1951, ApJ, 114, 407
- Strauss, F., Ducati, J. 1981, A&AS, 44, 337
- Ulmschneider, P. 1979, Space Sci. Rev., 24, 71
- von Braun, K., Chiboucas, K., Minske, J. K., Salgado, J. F., Worthey, G. 1998, PASP, 110, 810
- White, R., Basri, G. 2003, ApJ, 582, 1109
- White, R., Hillenbrand, L. 2004, ApJ, 616, 998